STUDY OF CHARACTERISTICS OF DRY FRICTION DAMPING

A.V. Srinivasan
B.N. Cassenti
D.G. Cutts

AD-A167 188

FINAL REPORT
April 1985

DTIC
ELECTE
APR 2 9 1986
D

Prepared for

AIR FORCE OFFICE OF SCIENTIFIC RESEARCH
Bolling AFB, Washington, DC 20332

CONTRACT F49620-83-C-0076

DTIC FILE COPY

AD-A167 188

REPORT DOCUMENTATION PAGE

1a. REPORT SECURITY CLASSIFICATION Unclassified	1b RESTRICTIVE MARKINGS		
2a SECURITY CLASSIFICATION AUTHORITY	3 DISTRIBUTION/AVAILABILITY OF REPORT Approved for public release; distribution unlimited.		
2b. DECLASSIFICATION/DOWNGRADING SCHEDULE			
4. PERFORMING ORGANIZATION REPORT NUMBER(S) R85-956479-2	5. MONITORING ORGANIZATION REPORT NUMBER(S) R85-956479-2 AFOSR-TR- 86-0164		
6a. NAME OF PERFORMING ORGANIZATION United Technologies Research Center	6b OFFICE SYMBOL (If applicable)	7a. NAME OF MONITORING ORGANIZATION AFOSR/NA USAF/AFSC	
6c. ADDRESS (City, State, and ZIP Code) Silver Lane East Hartford, CT 06108		7b. ADDRESS (City, State, and ZIP Code) Directorate of Aerospace Sciences Bldg 410, Bolling Air Force Base, DC 20332	
8a. NAME OF FUNDING/SPONSORING ORGANIZATION AIRFORCE OFFICE OF SCIENTIFIC Research	8b. OFFICE SYMBOL (If applicable) AFOSR/NA	9. PROCUREMENT INSTRUMENT IDENTIFICATION NUMBER F49620-83-C-0076	

8c. ADDRESS (City, State, and ZIP Code)	10 SOURCE OF FUNDING NUMBERS			
	PROGRAM ELEMENT NO	PROJECT NO	TASK NO.	WORK UNIT ACCESSION NO
BOLLING AFB, DC 20332	61102F	2302	B1	

11. TITLE (Include Security Classification)
Study of Characteristics of Dry Friction Damping

12 PERSONAL AUTHOR(S)
A. V. Srinivasan, B. N. Cassenti, D. G. Cutts

13a. TYPE OF REPORT Final Tech. Report	13b TIME COVERED FROM ____ TO ____	14 DATE OF REPORT (Year, Month, Day) April 1985	15 PAGE COUNT 45

16 SUPPLEMENTARY NOTATION

17	COSATI CODES		18 SUBJECT TERMS (Continue on reverse if necessary and identify by block number)
FIELD	GROUP	SUB-GROUP	Dry friction; damping; vibrations; structural dynamics.

19 ABSTRACT (Continue on reverse if necessary and identify by block number)

This report contains results of analytical and experimental efforts related to dry friction damping. A general time history solution is developed for a multi-degree-of-freedom system which incorporates the use of nonlocal laws of friction. The formulation and the solution are entirely nonlinear and have the necessary flexibility for modelling specific engineering problems where the presence of friction at interfaces influences the dynamics. Two examples are chosen to illustrate certain important aspects of the procedures.

A friction test assembly designed and fabricated under this program served as an experimental rig. The results from a limited number of tests are presented and discussed. A comparison between analytical and experimental results is given.

20 DISTRIBUTION/AVAILABILITY OF ABSTRACT ☐ UNCLASSIFIED/UNLIMITED ☒ SAME AS RPT ☐ DTIC USERS	21. ABSTRACT SECURITY CLASSIFICATION UNCLASSIFIED	
22a. NAME OF RESPONSIBLE INDIVIDUAL ANTHONY K AMOS	22b TELEPHONE (Include Area Code) (202) 767-4935	22c. OFFICE SYMBOL AFOSR/NA

This annual and final report covers the period between March 1, 1984 and April 30, 1985. The work reported here was under the sponsorship of the AFOSR under the technical direction of Dr. A. Amos.

Study of Characteristics of Dry Friction Damping

TABLE OF CONTENTS

PREFACE

This is the second of a two volume report on the subject of friction damping of dynamic systems. The first of these reports entitled "Study of Character- istics of Dry Friction Damping" was prepared as an annual report in March 1984 and submitted to the Air Force Office of Scientific Research.

The first report contained an introduction to the topic along with a thorough review of pertinent literature and discussion of (a) interface charac- teristics, (b) characterization of friction forces, (c) coefficient of friction and (d) dry friction damping technology. An analytical model and a corresponding experimental set up was also presented as the basis for further research. Possible modifications to a nonlocal law were also included. It is recommended that the reader study the first report prior to commencing the present volume, although this report is essentially self contained.

Accesion For		
NTIS CRA&I	☑	
DTIC TAB	☐	
Unannounced	☐	
Justification		
By		
Distribution /		
Availability Codes		
Dist	Avail and / or Special	
A-1		

SUMMARY

This report contains results of analytical and experimental efforts related to dry friction damping. A general time history solution is developed for a multi-degree-of-freedom system which incorporates the use of nonlocal laws of friction. The formulation and the solution are entirely nonlinear and have the necessary flexibility for modelling specific engineering problems where the presence of friction at interfaces influences the dynamics. Two examples are chosen to illustrate certain important aspects of the procedures.

A friction test assembly designed and fabricated under this program served as an experimental rig. The results from a limited number of tests are presented and discussed. A comparison between analytical and experimental results is given.

This annual and final report covers the period between March 1, 1984 and April 30, 1985. The work reported here was under the sponsorship of the AFOSR under the technical direction of Dr. A. Amos.

1. INTRODUCTION

One of the most important sources of energy dissipation in built-up struc-
tures pertains to dry friction at joints and at interfaces in contact with each
other. When materials with very low inherent damping are used in environments
offering essentially no aerodynamic damping (such as, for example, in space
structural systems), the ability of the structures to withstand resonant vibra-
tion depends almost entirely on the extent of friction damping. Even in the
design of components which can generate certain levels of aerodynamic damping, it
is essential to be able to estimate accurately the levels of non-aerodynamic
sources of damping because unlike the latter, the former can be either positive
or negative. For example, the aeroelastic instabilities of aircraft structures
such as airplane wings or turbomachinery blades are attributed to negative aero-
dynamic damping developing in the system as a result of its interaction with the
air forces causing the system to vibrate. In such situations, escalation of
vibratory stresses to dangerous levels is prevented only through the contribution
to damping from sources such as friction. In some instances, artificial devices
are designed and introduced into the structural system with the sole purpose of
developing friction forces leading to damping when the dynamics of the component
demands it. Thus, there is a clear need to enhance the level of understanding in
the broad area of dynamics of surfaces in contact.

Among the multitude of factors contributing to the dynamics of elastic
bodies in relative motion that come into contact with each other at interfaces,
the most significant factor is the governing law of friction. It is the law of
friction that accounts for the characteristics of contacting surfaces and the
environment; and establishes the relationship among forces and resulting motion.
The success of prediction of dynamic response of a structural component depends,
to a large extent, on the choice of a realistic friction law that accurately
portrays the interfaces. The laws of friction so constructed must be adaptable
in a dynamic analysis of the structural system and directly verifiable in a care-
fully controlled test.

This report is aimed at examining different characterizations of friction
forces at interfaces. A general nonlinear theory of dynamic systems is developed
in such a way that a local or nonlocal law guided by experimental data may be
incorporated. Solution procedures are presented and discussed.

This necessarily includes an extension of simple "local" characterization of
friction for the neighborhood of a single surface asperity to a "nonlocal" or
gross characterization for an interface having a large number of asperities.

Three laws of friction that are adaptable to dynamic analysis of structural
systems are outlined and discussed below.

1

2. LAWS OF FRICTION

One of the laws considered here is the simplest and represents the most commonly used form i.e.,

$$F = \hat{F} \ \text{sgn}(\dot{X})$$

This law is used when $|\dot{x}|$ is above a specified threshold of "sticking" and is replaced by a "static" friction condition if the relative velocity is below the threshold (this will be discussed further below).

A. Friction Force of Constant Amplitude

An application of this law for the system shown in Fig. 1 served as the basis for the parametric study leading to the design of an experimental rig. The latter will be discussed in a subsequent section but the highlights of the analysis are presented below.

The governing equation of motion for the system shown in Fig. 1 may be written as

$$M\ddot{x} + K(x-X) + F \ \text{sgn}(\dot{x}) + C(\dot{x}-\dot{X}) = 0 \quad \ldots \quad (2.1)$$

which may be written in a nondimensional form as

$$\ddot{q} + 2\zeta\xi\dot{q} + \zeta^2 q = -\ \text{sgn}(\dot{q})D - \frac{1}{\zeta^2}\ \ddot{f}(\tau) \ \ldots \quad (2.2)$$

where

$$q = \frac{M\omega^2}{KX_o} \ \bar{x}, \ \bar{x} = x-X, \ X = X_o f(\omega t), \ \tau = \omega t$$

The derivatives in Eq. 2.2 are with respect to τ.

$$\zeta = \frac{\omega_n}{\omega}, \quad \omega_n = \sqrt{\frac{K}{M}}, \quad D = \frac{F}{KX_o}, \quad F = \mu N \qquad (2.3)$$

$$\xi = \frac{C}{C_{cr}}, \qquad C_{cr} = 2\sqrt{KM}$$

The numerical solution of the governing differential equation 2 is obtained using the Newmark integration scheme (Ref. 1) with discrete time steps. The calculations are performed when the mass M is moving under the action of either a sinusoidal or step input displacement function. When the block is stuck (as indicated by the relative velocity dropping below a pre-specified threshold) static friction conditions are imposed. A test is then made at each time step to determine if the accelerating force on the block exceeds the static frictional force. As soon as this occurs, dynamic conditions are imposed and the motion parameters are calculated. A check on the magnitude of the velocity indicates whether or not the block has become unstuck. If the velocity threshold has not been exceeded, then static friction conditions are reimposed. This process is repeated until the block slips.

Two points are worthy of note in this type of solution. The first point pertains to the definition of the "stuck" condition. With the present approach, the friction force alternates as the velocity bounces within the specified threshold ($\pm$) region causing spurious acceleration spikes. The size of the velocity threshold has a marked effect on the response and guidelines may need to be obtained from test data. The second point is that the model permits incorporation of different friction models such as, for example, microslip in place of the "stuck" condition.

As stated earlier, the model was used in the design of the experimental setup. Figures 2 and 3 show typical results obtained.

These results were obtained using the parameters for the experimental rig i.e. the mass, spring, normal load, applied g loads etc. correspond to those used in the test. Figure 2 shows the input displacement and the resulting displacement, velocity and phase plane plot. The flat top in the output displacement characteristics, the nature of stick-slip motion evident in the velocity characteristic all lead to the stable limit cycle shown in Fig. 2. The kinks in the phase plane plot represent the displacements and velocities at which the system sticks and slips. Figure 3 shows the variation of friction force as a function of time, relative and absolute accelerations. The latter will be used in a later section of this report for making comparisons with measurement.

B. Friction Force Increasing with Relative Velocity

Another law that was examined in this study is of the form

$$F = F_o \tanh \frac{V_r}{V_o} \qquad (2.4)$$

This law has the advantage in that it degenerates into the simple law presented above or the familiar viscous law with appropriate assumptions. The single-degree-of-freedom system shown in Fig. 4, differs from that of Fig. 1 in that the spring and viscous damping forces relate to absolute motion of the masses rather than to motion relative to the frame. The equation of motion

$$M\ddot{x} + kx + c\dot{x} = F \quad \text{with} \quad V_r = \dot{a} - \dot{x}, \qquad (2.5)$$

can be solved numerically using a simple Euler integration scheme. Assuming

$$F_o = 0.1 \, Ka_o$$

$$\omega = 0.1 \, \omega_o, \, \omega_o = \sqrt{k/M}$$

$$V_o = 0.01 \, a_o\omega_o$$

$$C/C_o = 0.02$$

the computed response is shown in Fig. 5 for a typical cycle, indicating that the assumed friction law results in a high frequency ringing. An attempt was made to model an experimental set-up shown in Figs. 6 and 7, because test data from this set-up had shown responses with high frequency ringing (see Fig. 8). This had been attributed earlier to possible electronic noise. However, with the hyberbolic tangent law it was possible to reproduce these responses by modeling the experimental hardware as shown in Fig. 9. The elasticity in the dynamic system is allowed in the model. The equations governing the motion of this system are

$$m\ddot{X}_1 + c\dot{X}_1 + kX_1 = F$$

$$\qquad (2.6)$$

$$m\ddot{X}_2 + c\dot{X}_2 + kX_2 = P_o \sin \omega t - F$$

Again, the friction law was chosen to be

$$F = F_0 \tanh \frac{\dot{X}_0 - \dot{X}_1}{V_0} \qquad (2.7)$$

These equations were integrated using the Euler integration scheme and typical time histories of response are shown in Figs. 10, 11, and 12 for various forcing frequencies. The viscous damping, was chosen, as before, to be 2 percent critical with $F_0 = 0.1 \, P_0$, $V_0 = 0.01 \, P_0/\sqrt{Km}$ and $\Omega = \omega/\omega_0$. The ringing is clearly evident in the response coordinate X_1. The X_2 coordinate is a smooth sinusoid as it is being driven by the forcing function. As the forcing frequency approaches resonance, the ringing disappears but relative motion at the interface persists, resulting in damping. The results from this study show that modeling which takes into account the elasticity of the system may produce responses that are more realistic. Thus, in reducing data from complex structures care must be exercised so that certain responses may be recognized as inherent to the structural system rather than mere noise that should be filtered away.

C. Extension of Nonlocal Friction Law

Finally, the nonlocal law postulated by Oden and Pires (Ref. 2) and discussed in the first volume of this report (Ref. 3) has been extended to include velocity dependence for the forces at the interface and to integrate along the path followed by the points at the interfaces undergoing relative motion. Thus, the velocity dependence accounts for the dynamics of relative motion at interfaces and the type of integration proposed recognizes a nonisotropic weighting function. The nature of this extension is presented below.

Consider two surfaces, A and B, in relative motion and assume that surface B is stationary. The two surfaces may have many points in contact with each other at time t_1. Let X_1 be the surface coordinates on B. The subscript 1 refers to conditions when corresponding points in A and B are in contact with each other. Let $V_1(t)$ be the velocity of a point A in surface A that was initially in contact with B at time t_1 and position X_1. Then the relative motion of A may be written as

$$\vec{X}_{A_1} = \vec{X}_1 + \int_{t_1}^{t} \vec{V}_1 \, dt \tag{2.8}$$

The total distance travelled between t_1 and t is $R = \int_{t_1}^{t} |\vec{V}_1| \, dt$

$$\dot{R} = \begin{cases} |\vec{V}_1| & t \geq t_1 \\ 0 & t < t_1 \end{cases} \tag{2.9}$$

and

$$R = 0 \quad \text{at} \quad t = t_1$$

As stated earlier the point under consideration came into contact with a corresponding point in B at time t_1. As the point A moves over the contact surface a bond will develop. The adhesive strength will depend on the extent of time the two points were in contact with each other. The time of contact, in turn depends upon the relative speed of the two points at the time of contact. The adhesive strength will be proportional to the area of the bond. Let ϵ represent the dimension of the bond in the direction of motion. Before the two points come in contact $\epsilon = 0$. After they are in contact, they will deform together until the contact is broken. The growth of this bond by diffusion may be represented by an evolution law as follows

$$\dot{\epsilon}(x_1, t) = \begin{cases} 0 & t < t_1 \\ \dfrac{a_s}{|\vec{V}_1|} (\epsilon_o - \epsilon) + \dfrac{|\vec{V}_1|}{\ell_k} (\epsilon_k - \epsilon) & t \geq t_1 \end{cases} \tag{2.10}$$

where a_s, ℓ_k, ϵ_o, ϵ_k are constants that can be chosen to represent a given situation where either the static (subscript s) or kinematic (subscript k) condition is expected to be predominant. The above form is chosen to allow for the realistic growth of bond both at low and high relative velocities.

This is illustrated by considering the steady state value for ϵ which are given by

$$\dot{\epsilon} = 0$$

or

$$\epsilon = \frac{\dfrac{a_s}{|\vec{V}_1|}\,\epsilon_o + \dfrac{|\vec{V}_1|}{\ell_k}\,\epsilon_k}{\dfrac{a_s}{|\vec{V}_1|} + \dfrac{|\vec{V}_1|}{\ell_k}} \tag{2.11}$$

For low speeds, (i.e., V_1 very small),

$$\frac{a_s}{|\vec{V}_1|} \gg \frac{|\vec{V}_1|}{\ell_k} \quad \text{and} \quad \epsilon \approx \epsilon_o$$

For high speeds

$$\frac{a_s}{|\vec{V}_1|} \ll \frac{|\vec{V}_1|}{\ell_k} \quad \text{and} \quad \epsilon \approx \epsilon_k \tag{2.12}$$

The constants a_s and ℓ_k can be used to account for the effect of temperature on the rate of bond growth, i.e., if T_{S_1} is the surface temperature at A_1, and T_a and T_ℓ are activation energies then

$$a_s = a_o e^{-T_a/T_{S_1}}$$

$$\ell_k = \ell_o e^{T_\ell/T_{S_1}} \tag{2.13}$$

will account for the rate of bond growth.

As relative motion begins and the two points move apart, the shear force at the bond will change. At first, the shear force will increase, reach a maximum, and as the bond continues to break, the force will decrease. The above characteristics can be represented by a function ϕ as follows

7

$$\phi = \phi(R/\epsilon) = \frac{1}{\Gamma(p+1)} (R/\epsilon)^p e^{-(R/\epsilon)} \qquad (2.14)$$

It may be noted that the ratio R/ϵ represents the relative length of motion in terms of bond length. This function is shown in Fig. 13 for several values of the parameter p. R is along the path of motion and is ≥ 0 by definition. Hence ϕ is finite if $p > -1$ which requires $p > -1$.

Perpendicular to the path, a second weighting function is allowed to represent the bond area. This has been taken to be (see Fig. 14)

$$W\left(\frac{\eta}{\rho}\right) = \frac{e^{-(\eta^2/2\rho^2)}}{\sqrt{2\pi}} \qquad (2.15)$$

where η is the distance perpendicular to the path. The shear force acting between the two points is now made proportional to the product of ϕ and W. Further, the strength of the bond must also depend upon the normal stress $\sigma_n(x_1)$ at x_1. Therefore, the proposed nonlocal law for the shear force at x_1 is essentially complete with the following representation

$$\vec{\tau}(\vec{X}) = \mu_s \int_{-\infty}^{\infty} \int_{-\infty}^{\infty} \phi(R/\epsilon) W(\eta/\rho) \sigma_n(\vec{X}_1) \frac{dX_1 dy_1}{\epsilon_0 \rho} \qquad (2.16)$$

Recognition of the fact that the frictional shear at X will be in a direction opposite to the relative displacement $\vec{u}$ completes the required representation as follows

$$\vec{\tau}(\vec{X}) = -\mu_s \int_{-\infty}^{\infty} \int_{-\infty}^{\infty} \phi(R/\epsilon) W(\eta/\rho) \sigma_n(\vec{X}_1) \frac{\vec{u}}{|\vec{u}|} \frac{dX_1 dy_1}{\epsilon_0 \rho} \qquad (2.17)$$

It will be shown that the constants present in this formulation can be related to the static and kinetic coefficients of friction. Consider the surface A moving at a constant velocity relative to B under a constant normal stress. Then, it can be shown that

$$\vec{\tau}(\vec{X}) = -\mu_s \frac{\vec{V}}{|\vec{V}|} \left(\frac{\epsilon}{\epsilon_o}\right) \sigma_n \qquad (2.18)$$

where $\vec{V}$ is the relative velocity. Clearly the above is a degeneration of the general representation to a local law.

For slow speeds $\epsilon \approx \epsilon_o$ and then

$$\vec{\tau}(\vec{X}) \approx -\mu_s \frac{\vec{V}}{|\vec{V}|} \sigma_n \qquad (2.19)$$

μ_s can be identified with the static coefficient of friction. For high velocities $\epsilon \approx \epsilon_k$

and

$$\vec{\tau}(\vec{X}) \approx -\mu_s \frac{\vec{V}}{|\vec{V}|} \left(\frac{\epsilon_k}{\epsilon_o}\right) \sigma_n \qquad (2.20)$$

Hence the quantity $\mu_s \dfrac{\epsilon_k}{\epsilon_o}$ can be identified with the kinetic coefficient of friction

i.e.,

$$\mu_k = \mu_s(\epsilon_k/\epsilon_o)$$

$$\qquad (2.21)$$

$$\epsilon_k = \frac{\mu_k}{\mu_s} \epsilon_o$$

3. DYNAMICS OF STRUCTURAL SYSTEMS WITH INTERRUPTED INTERFACES

A general structural system with an arbitrary number of interfaces is considered. The friction forces developing at these interfaces during vibration are treated in such a way that the influence of different laws of friction may be examined. The solution procedure leads to a calculation of time history of the vibratory motion either under arbitrary transient loading or as the driving frequency is swept over a given range so that the dynamic response as well as the nature of its stability can be evaluated.

A. Formulation

The governing equations of motion for the structural system may be represented in matrix form as

$$[m]\{\ddot{x}\}+[c]\{\dot{x}\}+[k]\{x\} = \{f\}+\{F\} \qquad (3.1)$$

$\{x\}$ represents physical displacements

$\{f\}$ represents forces of friction

$\{F\}$ represents external forces

$[m]$, $[c]$ and $[k]$ are the mass, damping, and stiffness matrices.

It may be noted that some of the elements of $\{f\}$ and $\{F\}$ may be zero. Also, if $\{f\}$ represent forces at internal interfaces only, the arithmetic sum of two elements of $\{f\} = 0$.

Let $[\Phi]$ represent the matrix of eigenvectors $\{\varphi\}$ obtained from the solution of equation (3.1) in which $[c]=0=\{f\}=\{F\}$ and $[\omega^2]$ represents the corresponding eigenvalues.

Successive transformations, as shown below, can lead to

$$\{\ddot{z}\} + [\omega^2]\{z\} = \{g\}+\{G\}-[H] \qquad (3.2)$$

where

$$\{z\} = [\phi]^T\{y\}$$

$$\{y\} = [\sqrt{m}]\{x\}$$

$$\{g\} = [\phi]^T[\ 1/\sqrt{m}\ ]\{f\} \tag{3.3}$$

$$\{G\} = [\phi]^T[\ 1/\sqrt{m}\ ]\{F\}$$

$$[H] = [\phi]^T[c][\phi]\{\dot{z}\}$$

The elements of $\{G\}$ are functions of time and the elements of $\{g\}$ represent the nature of friction forces.

The ith row of Eq. (2) can be written as

$$\ddot{z}_i + \omega_i{}^2 z_i = g_i + G_i - h_i \tag{3.4}$$

$g_i = g_i(z_i, \dot{z}_i)$ in view of Eq. (3.3) represents the influence of friction forces in mode i;

$G_i = G_i(t)$ represents the generalized force in the ith mode and

$h_i = h_i(\dot{z}_i)$ represents the influence of viscous type damping forces in the ith mode.

B. Solution

The solution to Eq. (3.4) can be written in terms of the complementary solution and the particular integral, i.e., $z = z^C + z^P$

$$z_i{}^C = C_i^{(1)} e^{i\omega_i t} + C_i^{(2)} e^{-i\omega_i t} \tag{3.5}$$

where the constants $C_i^{(1)}$ and $C_i^{(2)}$ are determined from the initial conditions.

11

The particular solution is assumed to be

$$z_i^P = D_i^{(1)}(t)e^{i\omega_i t} + D_i^{(2)}(t)e^{-i\omega_i t} \tag{3.6}$$

$$\dot{z}_i^P = \dot{D}_i^{(1)}(t)e^{i\omega_i t} + \dot{D}_i^{(2)}(t)e^{-i\omega_i t} + i\omega\left\{D_i^{(1)}(t)e^{i\omega_i t} - D_i^{(2)}(t)e^{-i\omega_i t}\right\} \tag{3.7}$$

As only one function can be arbitrary in the solution of Eq. (3.4), a relationship between $D_i^{(1)}$ and $D_i^{(2)}$ can be obtained by setting

$$\dot{D}_i^{(1)}d^{i\omega_i t} + \dot{D}_i^{(2)}e^{-i\omega_i t} = 0 \tag{3.8}$$

Thus,

$$\dot{z}_i^P = i\omega\left\{D_i^{(1)}(t)e^{i\omega_i t} + D_i^{(2)}(t)e^{-i\omega_i t}\right\} \tag{3.9}$$

Differentiating Eq. (9) once more to obtain $\ddot{z}_i^P$ and substituting in Eq. (3.4) leads to a solution for $D_i^{(1)}$ and $D_i^{(2)}$.

$$\begin{aligned}
z_i = &\; C_i^{(1)}\,e^{i\omega_i t} + C_i^{(2)}\,e^{-i\omega_i t} \\
&- \frac{i}{2\omega_i}\int_o^t \left(g_i + G_i - H_i\right)e^{i\omega_i(t-\tau)}d\tau \\
&+ \frac{i}{2\omega_i}\int_o^t \left(g_i + G_i - H_i\right)e^{-i\omega_i(t-\tau)}d\tau
\end{aligned} \tag{3.10}$$

where $g_i = g_i\{z_i(\tau), \dot{z}_i(\tau)\}$

$H_i = H_i\{\dot{z}_i(\tau)\}$

$G_i = G_i(\tau)$

It may be noted that $C_i^{(1)}$ and $C_i^{(2)}$ are calculated from prescribed initial conditions, i.e., $\{x\}$ and $\{\dot{x}\}$ at $t = 0$. With $\{x\}$ and $\{\dot{x}\}$ prescribed at $t = 0$, z_i can be calculated from Eq. (3); i.e.,

$$\{z\}_{t=0} = [\phi]^T[\sqrt{m}]\{x\}_{t=0}$$

$$\{\dot{z}\}_{t=0} = [\phi]^T[\sqrt{m}]\{\dot{x}\}_{t=0}$$

which transforms the physical coordinates to modal coordinates.

C. Numerical Application

The implicit integration procedure (Eq. (3.10)) described above has been coded on a P.C. (HP9816) and several example problems were run to verify the procedure and the program. Only two examples are shown below to illustrate certain aspects of the procedure including important computational steps that need special attention in obtaining reliable results.

1. Single-Degree-of-Freedom Example

The numerical solution of a simple single degree of freedom system with a Coulomb type of friction interface (Fig. 4) is the first example. With the initial conditions prescribed as $x = x_0$, $\dot{x} = 0$ at $t = 0$, the solution of the governing equation $m\ddot{x} + kx = -f \, \text{sgn}(\dot{x})$, subjected to the above initial conditions can be shown to be

$$x = \begin{cases} \left\{ x_0 - (2N+1)\dfrac{F}{k} \right\} \cos \omega_0 t + (-1)^N \dfrac{F}{k} & N < N_0 \\[2em] (-1)^{N_0} \left\{ x_0 - 2N_0 \dfrac{F}{k} \right\} & N \geq N_0 \end{cases} \qquad (3.11)$$

where N = number of half cycles completed, truncated to the greatest integer less than

$$\frac{\omega_0 t / \pi}{}$$

and $\quad N_0 = \frac{1}{2} \left(\frac{kx_0}{F} - 1 \right)$

Figure 15 shows the time history of motion obtained by numerical integration which is identical to the exact solution at all times until the mass comes to rest at $t = \frac{\pi N_0}{\omega_0} \sim 11$ units of time as shown in Fig. 15. Beyond this time, a very slight tendency to oscillate is indicated.

The results from this example confirmed that the code is able to calculate highly nonlinear conditions with acceptable accuracy.

2. Two-Degree-of-Freedom Example

The second example chosen is a two-degree-of-freedom system which tests some important aspects of frictionally damped systems as discussed below.

Figure 16 is the analytical model of a 2D.O.F. which has a rigid body mode and a flexible system mode. When mass 2 is stuck, the system degenerates into the S.D.O.F. model discussed above. With $P = P_0 \sin \omega t$ and an assumed friction force of $\mu N = 3P_0$, the system would respond as a S.D.O.F. as long as the driving frequency is not close to the natural frequency, $\sqrt{K/m}$. At a frequency close to the natural frequency, the spring force would gradually build up to overcome $3P_0$ and mass 2 will slip. However, at $\omega = 1.14 \sqrt{K/m}$ and $\mu N = 3P_0$, calculations were made using the displacement at each time as the criteria for convergence. The resulting time history for the displacement of mass 2 and the friction force at the interface are shown in Figs. 17 and 18 respectively. These results are unacceptable: the mass 2 cannot begin to move because the friction force at the interface has not reached $3P_0$ as can be seen from Fig. 18. This is an illustration of the influence of numerical analysis on the solution and suggests the need to exercise considerable care in the choice of convergence criterion.

The convergence criterion was changed to a check on velocity at each step and the results show some improvements as can be observed from Figs. 19 and 20. Mass 2 moves but there is no steady drift. However the frictional force is quite erratic. This is an important problem that points to erroneous results that demand a careful look into modeling friction dependent systems.

3. Simplified Nonlocal Law

A final attempt was made by using a simplfied version of a nonlocal law as shown below

$$
\dot{F} = \begin{cases} -\dfrac{\mu N}{\epsilon}\, \dot{x} & |F| < \mu N \\[2em] 0 & |F| > \mu N \end{cases} \tag{3.12}
$$

Convergence criterion based on velocities was used and the results obtained are shown in Figs. 21 and 22. Clearly, the displacement of mass 2 is essentially zero until the required friction force exceeds μN. Although the friction force shows some instability, the representation is superior to that seen earlier in Fig. 20.

These examples illustrate the complexity of modeling friction at interfaces, even for relatively simple systems. Representation of the friction law as well as numerical methods have to be chosen with utmost care.

4. EXPERIMENTAL PROGRAM

A. Configuration

The photographs of the test assembly are shown in Figs. 23 and 24. Figure 24 shows the details of the test pieces. The entire friction assembly is mounted on a slip plate connected to the shaker so that predetemined acceleration inputs may be applied to the system. The springs (threaded rods connected to flexures; the latter are cantilever beams to the tips of which the threaded rods are connected) offer resistance to motion of the loaded mass and friction forces manifest at the interfaces. The normal load on the block may be varied by changing the weight hanging from the block.

The system had been designed such that the natural frequency of vibration for the translational (axial) mode of interest would lie between 100 and 150 Hz.

Details of the titanium test pieces are shown in Fig. 25. The actual friction surfaces are 6 mil hardface coatings of tungsten carbide, as shown.

B. Preliminary Modal Analysis

A preliminary modal analysis was performed to examine the dynamics of the system after it was assembled in place. The predominant mode of the system is, as designed, one of translation (see Fig. 26) occurring around 143 Hz, although a negligible amount of pitching and yawing modes can be present, especially when the friction interfaces are disengaged. There is a "rocking" mode of the mass at around 73 Hz with axial amplitudes considerably less than that at the mode of interest. Damping in the axial mode was predicted to be ~0.003 based on a multi-degree-of-freedom fit of the frequency response function.

A lateral yawing mode was found at 129 Hz and could have compromised results if there had been any significant asymmetry in the friction forces. This did not prove to be the case in the subsequent testing.

Upon completing the assembly with friction interfaces in place, but with an external normal load of 26# on the loading cable, the modal analysis was repeated and the results are shown in Fig. 27. The "rocking" and "yawing" modes have been suppressed; the mode of interest was found to be almost critically damped in the vicinity of 148 Hz.

C. Test Procedure

Exploratory sweeps between 130 and 160 Hz at low acceleration (< 5g) were made to examine system response characteristics. The 4g level was found to be a critical one at all frequencies since the response acceleration waveform became distorted due to the onset of slipping conditions. The input level was found to be the more sensitive parameter and hence a procedure was selected which required the input level to be increased gradually in steps while the frequency was held constant. This was performed at four frequencies namely, 135, 143, 150 and 155 Hz. The input level was varied from the level at which slipping was initiated, until either a divergent condition or 10 g occurred. The input acceleration, moving-block absolute acceleration and flexure strain gage output were recorded on a visicorder. A separate static test was performed to determine the constant of proportionality to convert the strain gage conditioner output to relative displacement of the moving block. The constant was found to be approximately 1 volt per 0.001 inch.

D. Test Results

Typical traces of the input and responses for slipping conditions are given in Figs. 28 and 29. Figure 28 shows the responses at 135 Hz/6g input and Fig. 29 shows the response for 143 Hz input frequency at 5g and 8g levels. At the 8g level a stable and an unstable condition (which occurred without warning) are shown.

The friction surfaces were characterized before and after the series of tests by means of a Sloan Dektak II profilometer. Figure 30 shows the asperity profiles before the test series in the x and y directions, and Fig. 31 the changed profiles taken after the tests. The before-test profiles show an important component of 80 micron scale with an amplitude of 13 to 18 microns, apparently isotropic in the x, y coordinates. After test, the 80 micron scale asperities are still visible but of much smaller amplitude, and with a smaller amplitude in the x direction (the direction of sliding).

The response at resonant frequency to an input displacement of $Xo = .0002$ ft in amplitude (5g equivalent acceleration) is shown in Figures 2, 3, 32 and 33 where these responses are shown in dimensionless form. Since the term $M\omega^2/K$ in equation 2.3 becomes equal to 1 at a resonance with small damping, $\bar{x} = q\, Xo$. From Figure 2, $q = .15$; therefore $\bar{x}$ becomes .00003 ft or .00036 inches, comparing well with the measured value of .00023 inches in Table 1 (5g/143 Hz). This is a good agreement considering the critical nature of the response at the undamped resonant frequency of the system.

At resonance, the value of $\ddot{x}M/KX_o = 1$ as can be seen from Figure 3. This can be solved for x leading to a value of 5g for the absolute acceleration, comparing closely with the 6g in Table 1. The response was also computed for equivalent 4g and 8g input accelerations. In the 4g case no slipping occurred and in the 8g case divergence of the response occurred. This compares favorably with the results obtained from tests (see Table 1).

5. CONCLUSIONS

The following observations summarize the principal findings from the tests as well as from a comparison between test data and corresponding analysis. These observations are to be understood as valid for the frequency and g level ranges tested. It must be noted that the measured acceleration is absolute and is compared with corresponding calculation. Relative acceleration from the calculations is also shown.

1) Slipping at the interfaces occurs at and above a certain g level independent of the excitation frequency (see Table 1).

2) Above a certain g level the amplitudes of relative slip motion experienced divergence limited entirely by nonlinearities due to the increase in flexure stiffness at large amplitude.

3) As the mass undergoes sticking and slipping the resulting accelerations are sudden and large. This creates an impulse type of input which in turn induces higher frequency responses seen as ringing (See Fig. 28 and 29).

4) Responses can be nearly sinusoidal above certain g levels.

5) Rubbing was observed to have occurred only on a portion of the total area of contact. It is likely that the engaging surfaces were not perfectly aligned due to machining tolerance.

6) As the input displacement reaches a maximum (Fig. 28, 32), provided the g level is sufficiently high, slipping begins to occur and reaches a maximum somewhat later than the time at which the input acceleration reaches its maximum.

7) As the input displacement is returning to zero upon completing the first half cycle, the relative motion at the interfaces remains constant (i.e. the masses are stuck).

8) As the input displacement continues to increase beyond the first half cycle, the masses begin to experience relative slip again and try to follow the input, although lagging.

9) At the instant of sticking, the velocity suddenly drops to zero (Fig. 2) from a finite value, resulting in a sudden increase in acceleration. This is shown by large discontinuities in the acceleration traces. Where the discontinuities appear several times, the interpretation is that local stick-slips continue until a full slip occurs.

10) No ringing of high frequency response is evident in the analytical
results since the model is merely a single-degree-of-freedom system.

REFERENCES

1. Bathe, K.-J.: Finite Element Procedures in Engineering Analysis, Prentice-Hall, Inc. 1982. See Section 9.2.4: The Newmark Method.

2. Oden, J. T. and Pires, E. B.: Nonlocal and Nonlinear Friction Laws and Variational Principles for Contact Problems in Elasticity. J. App. Mech., Vol. 50, 1983.

3. Srinivasan, A. V.; Cassenti, B. N. and Cutts, D. G.: Study of Characteristics of Dry Friction Damping, Annual Report R84-956479-1, March 1984.

TABLE 1

MEASURED RESPONSES OF MOVING BLOCK FOR SINUSOIDAL INPUT AT BASE

INPUT FREQ (Hz) / ACCEL (g)	SYSTEM RESPONSE: ABS ACC (g)/ REL DISP (mil)					
	135	143	150	155	135 (Repeat)	143 (Repeat)
4.0	5.8/.25	5.0/.08	5.1/*	5.0/*	6.0/*	4.9/*
5.0	8.4/.44	6.0/.23	5.8/*	5.9/*	6.5/*	6.6/*
6.0	9.5/.30 U	10.0/.33	7.9/*	7.6/*	8.2/*	9.5/*†
7.0	11.5/.55 U	11.5/.50	9.0/*	10.0/*		10.9/*
8.0		U	12.0/*	11.6/*	12.0/*	12.5/*
ONSET OF SLIP INPUT ACC(g)	3.8	3.9	4.0	4.2	4.2	4.0

NOTE: U = UNSTABLE CONDITION

* No Data due to strain gage failure during earlier instability
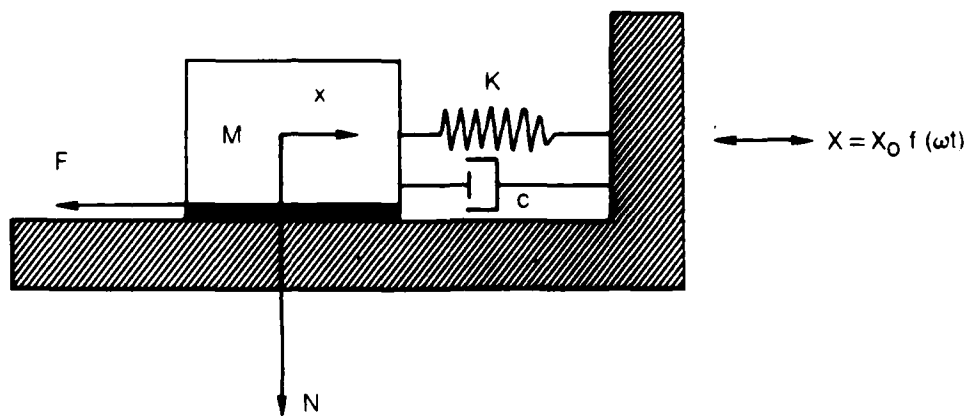
Fig. 1 S.D.O.F. System Damping Model

$X = X_0 \, f \, (\omega t)$
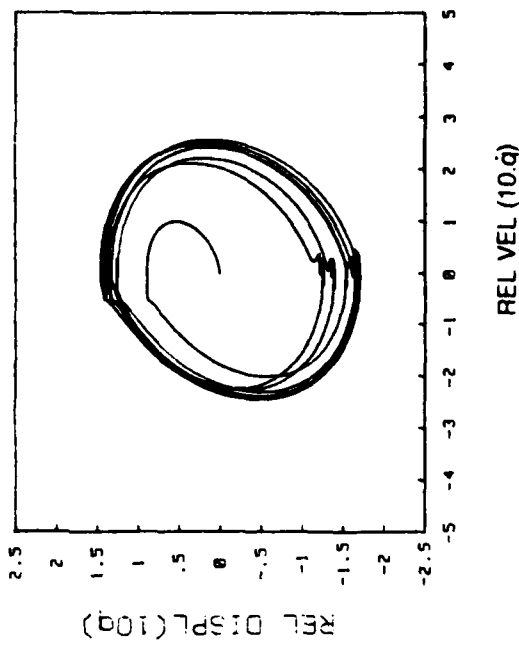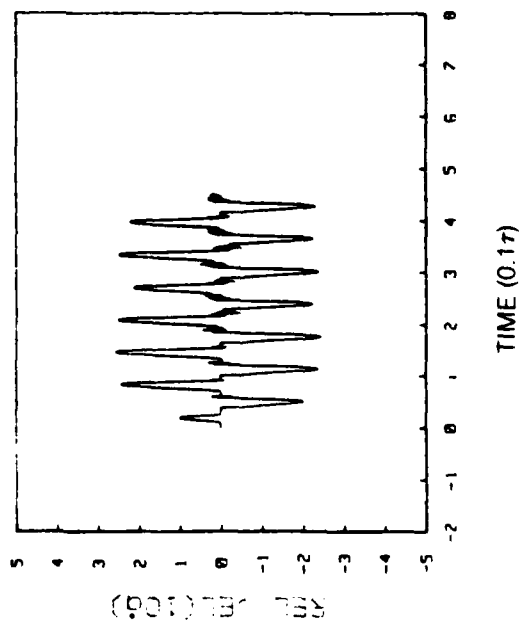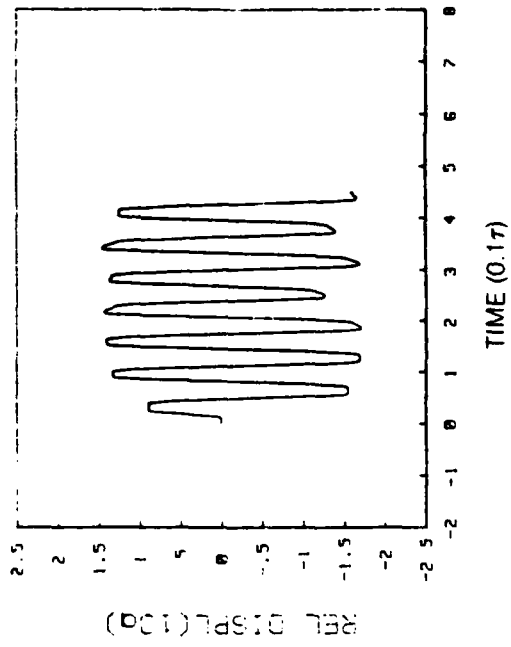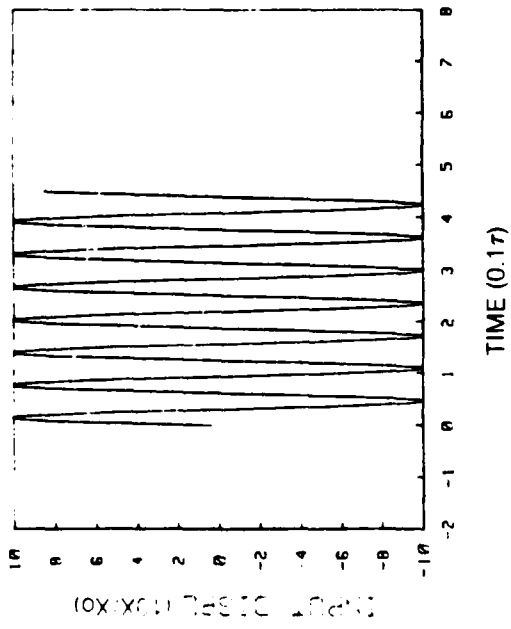
Fig. 2 Analysis of S.D.O.F. System
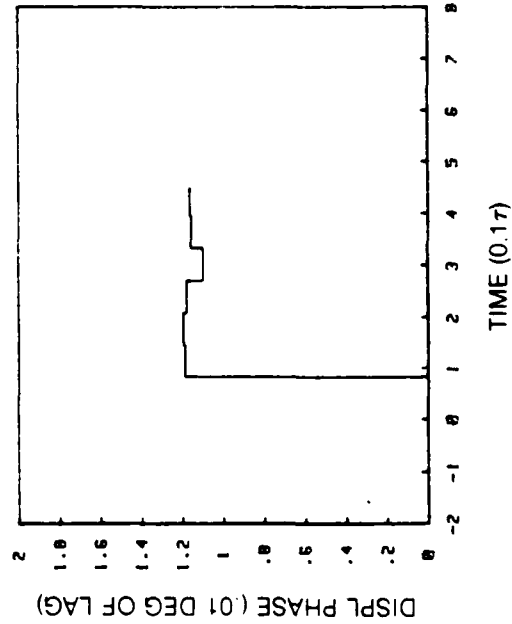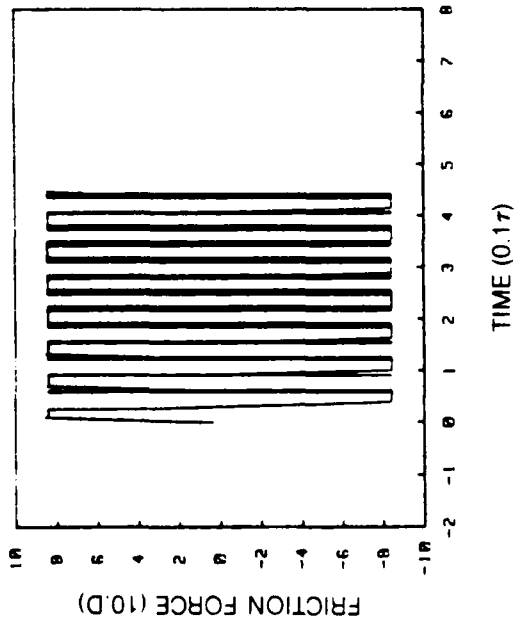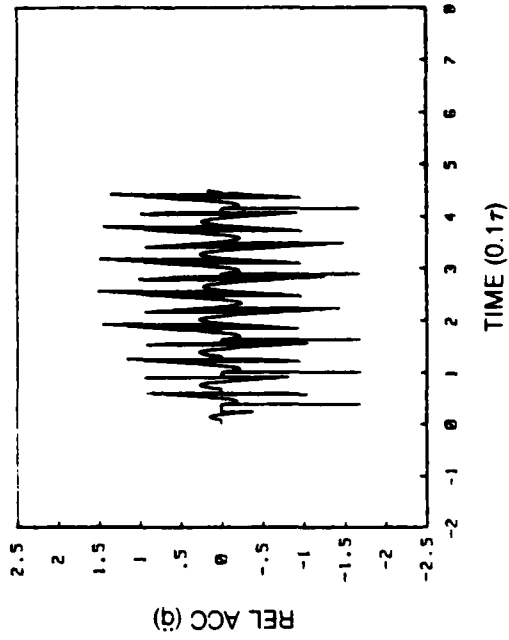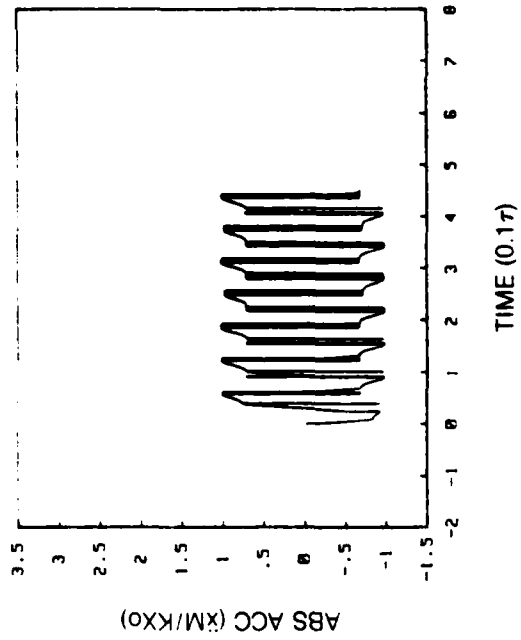
Fig. 3 Analysis of S.D.O.F. System (Continued)

85-4-55-11
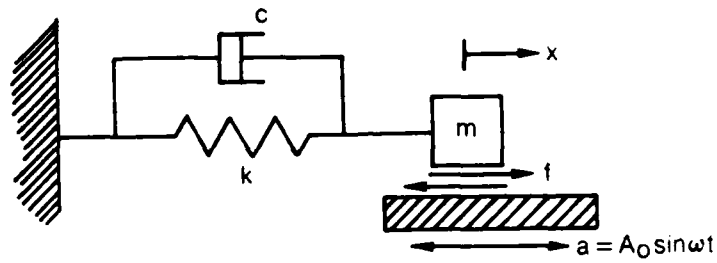
Fig. 4 A Single Degree-of-Freedom Model of an Experimental Step
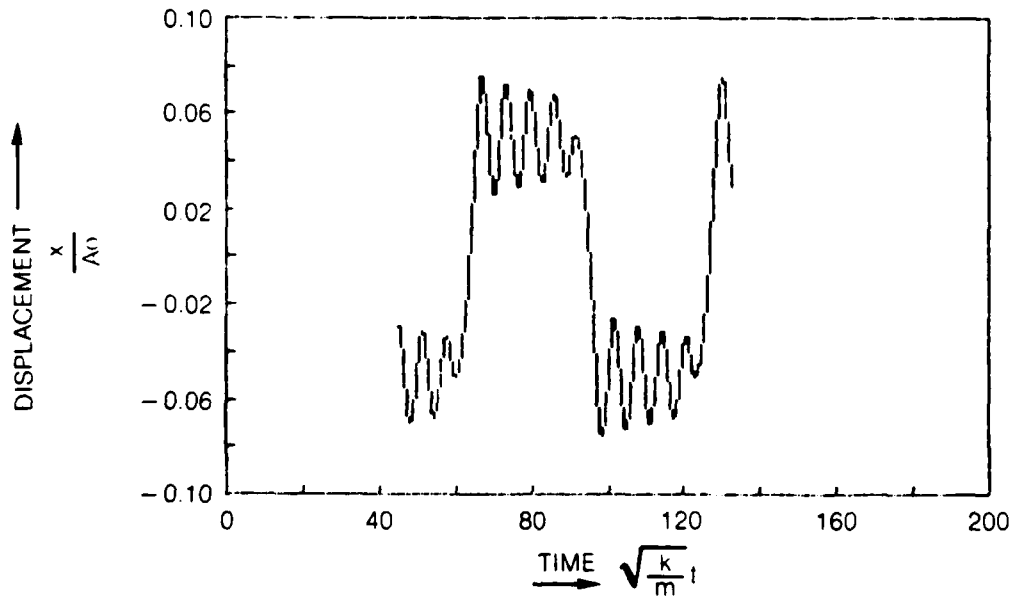
Fig. 5 Typical Response Calculated for the Model of Fig. 4

LOADING PLATFORM

UPPER ARM

ACCELEROMETER

LOAD BOLTS

STATIONARY UPPER
TEST PIECE

PIVOT
BEARING

MOVING LOWER
TEST PIECE

INPUT CONTROL
ACCELEROMETER

SLIP PLATE ATTACHED
TO SHAKER

CLAMP BLOCK
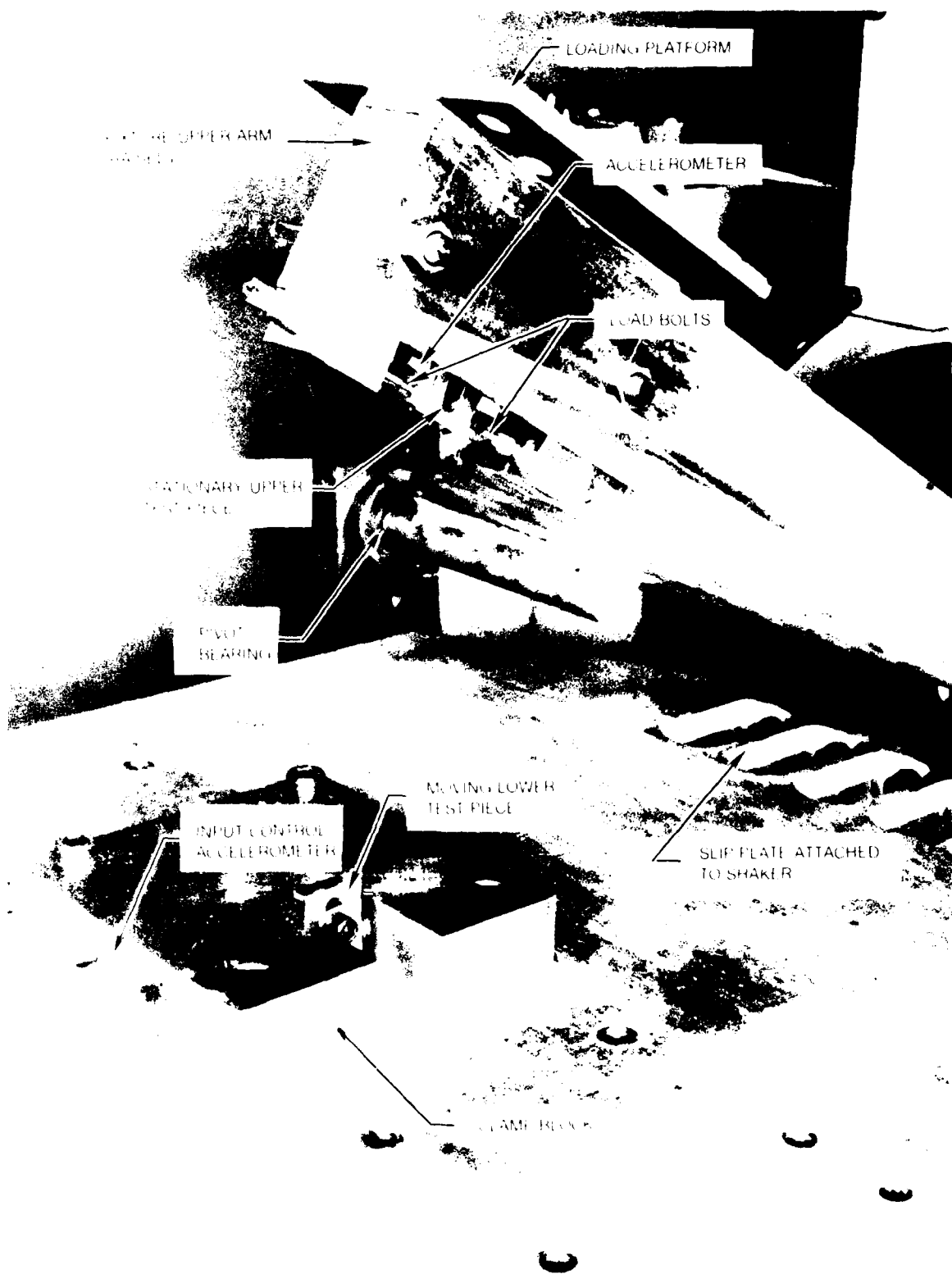
Fig. 6 Friction Test Assembly (Upper Arm Raised)

Fig. 7 Friction Test Assembly

7188-A

81-3-7-48

FREQUENCY: 140 Hz
INPUT ACCEL: 5g pk
HORIZ AXIS: 0.0127 mm/div
VERT AXIS: 115.2 N/div

271 N
494 N   APPLIED NORMAL LOAD
672 N

FREQUENCY: 280 Hz
INPUT ACCEL: 20g pk
HORIZ AXIS: 0.032 mm/div
VERT AXIS: 115.2 N/div

MEASURED FORCE

INPUT ACCELERATION
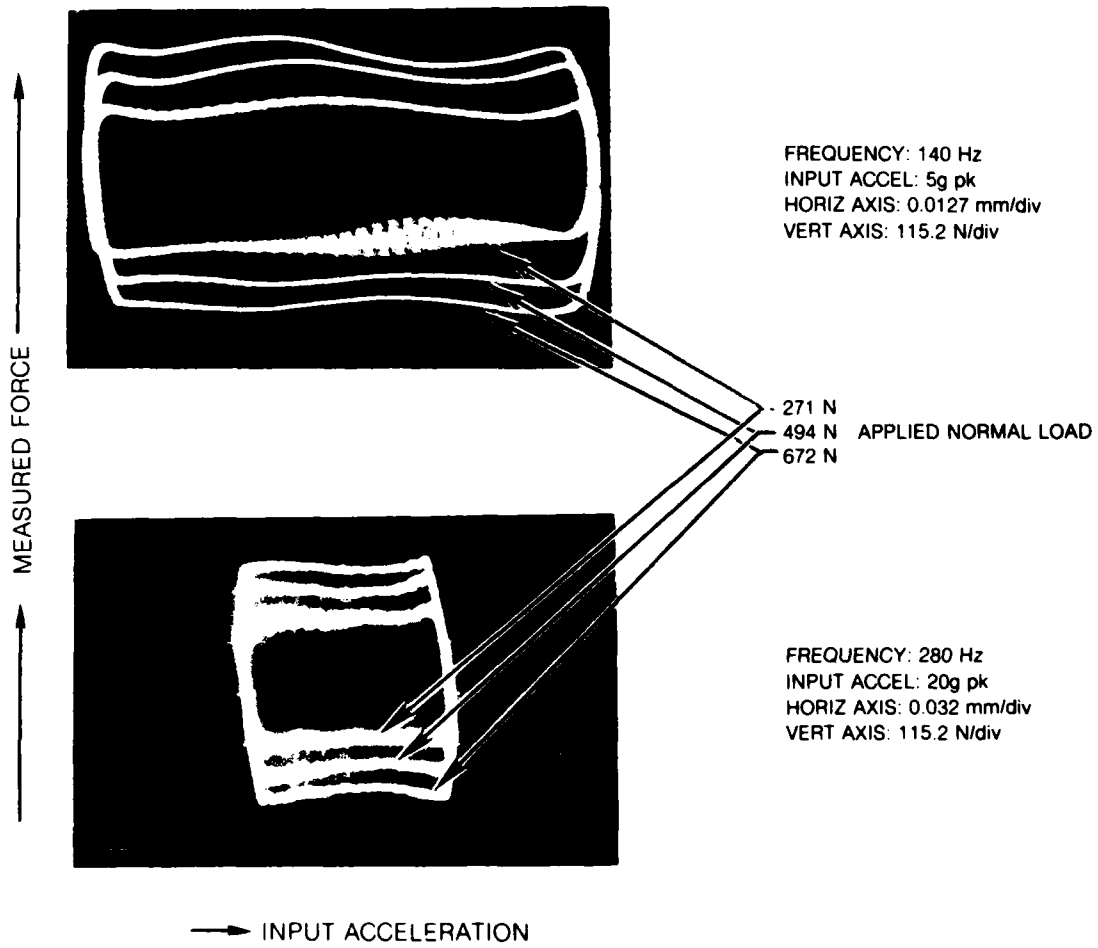
Fig. 8 Typical Measured Friction Force — Slip Loops
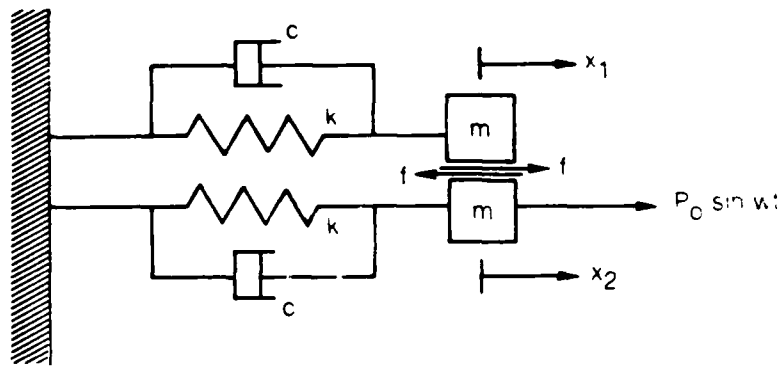
Fig. 9 Two Degree of Freedom Model
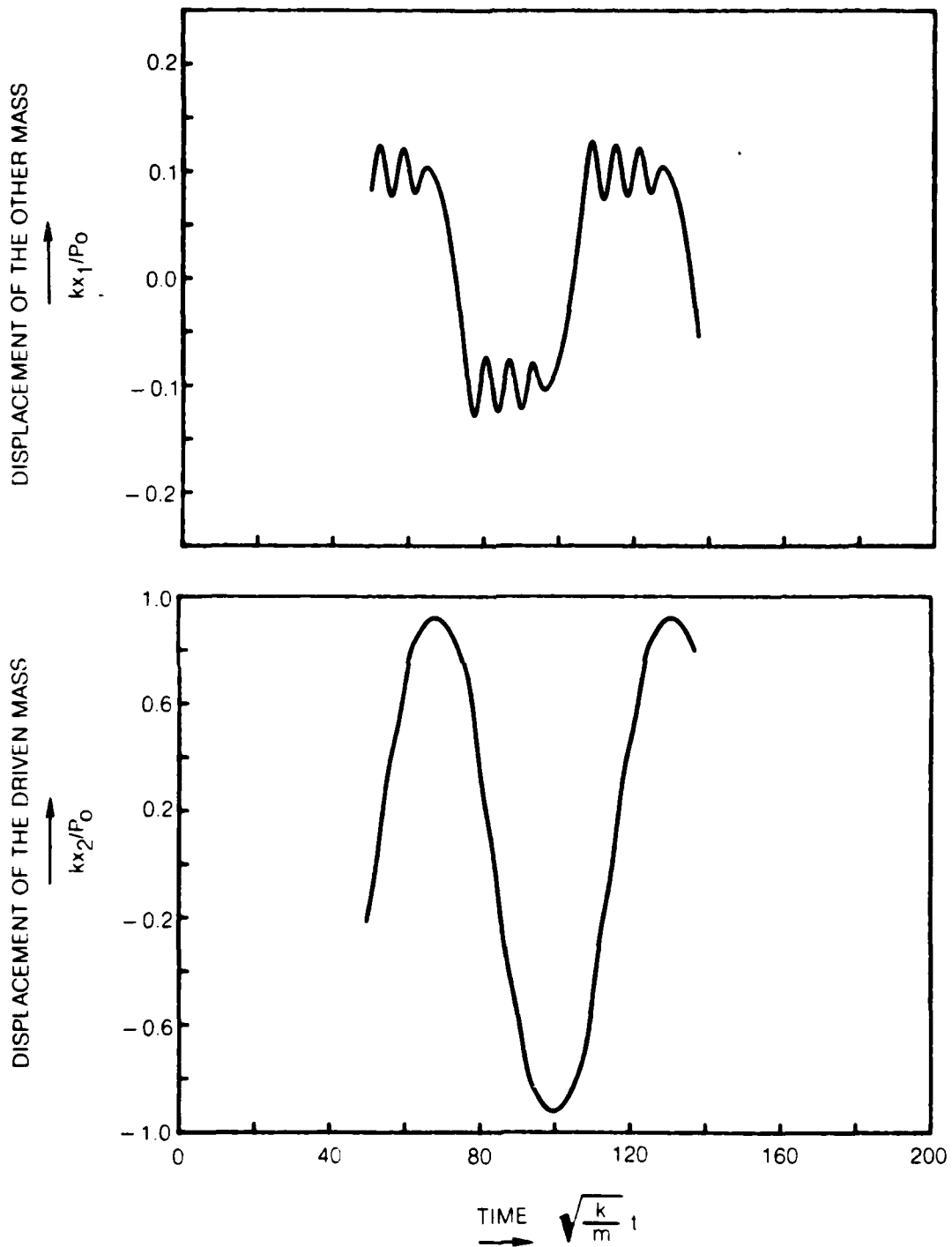
Fig. 10 Analytical Response for Two Degree of Freedom System of Fig. 9 ($\Omega = 0.1$)

85-4-69-4
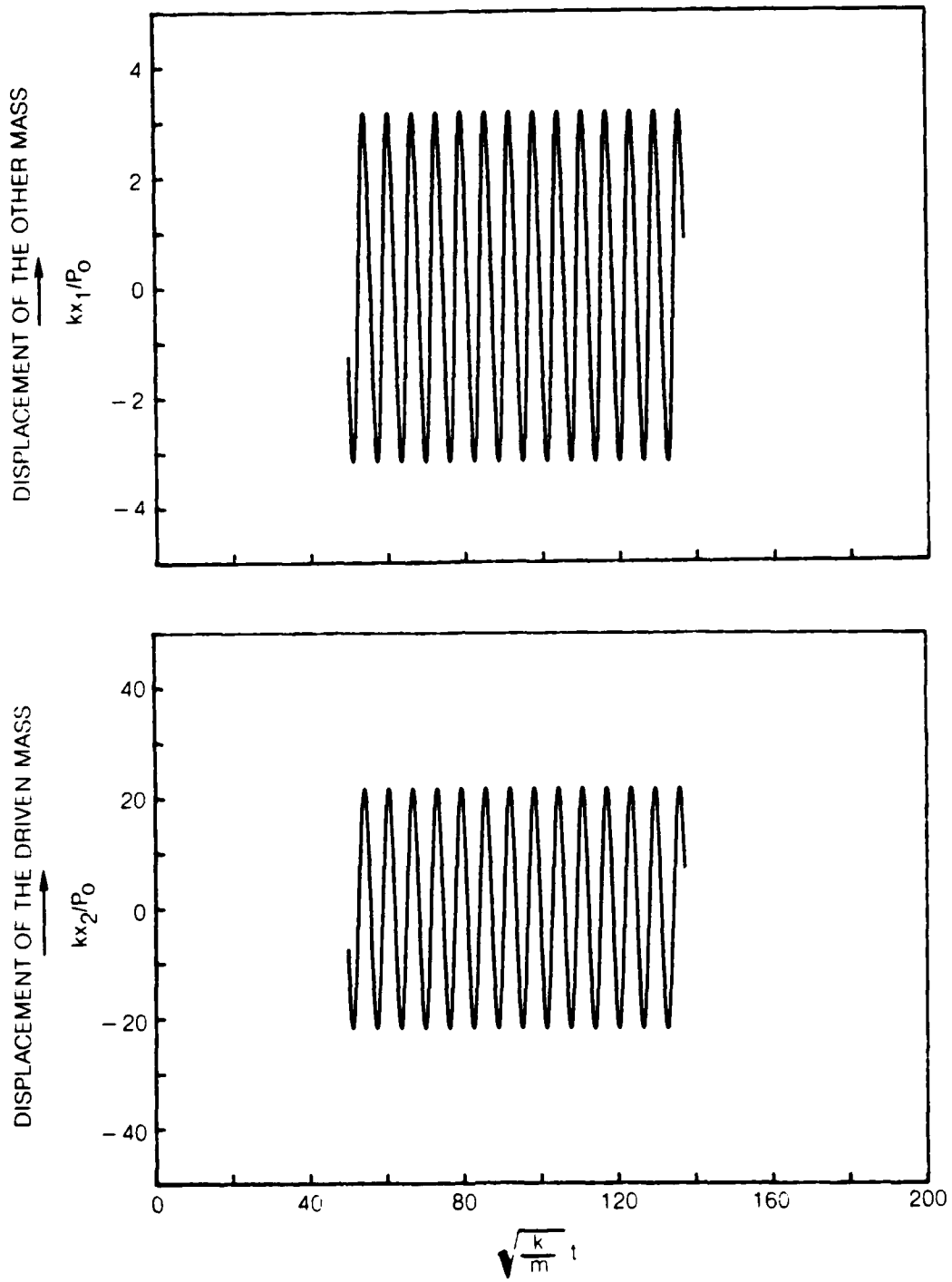
Fig. 11 Analytical Response for Two Degree of Freedom System ($\Omega = 1.0$)
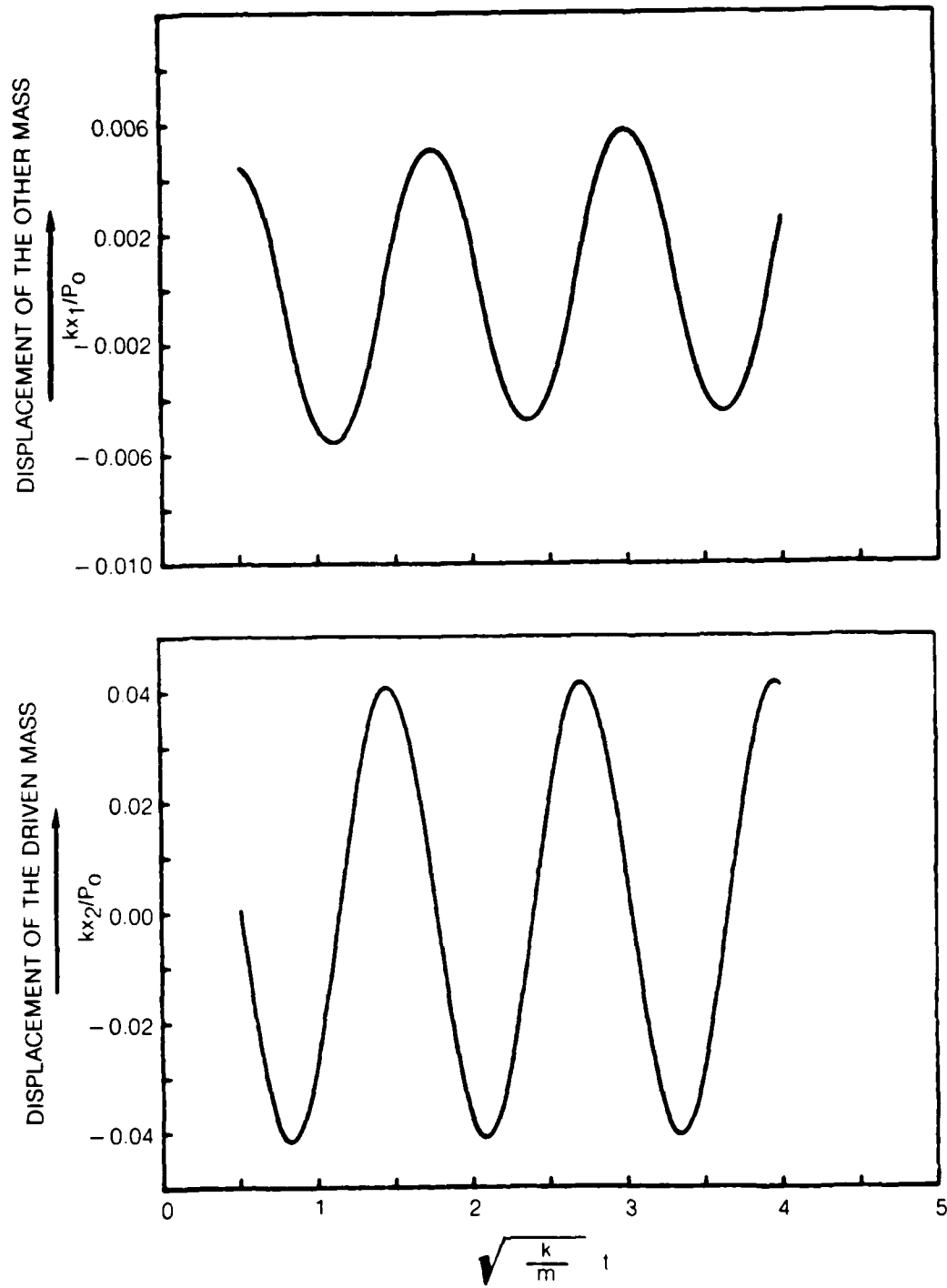
Fig. 12 Analytical Response for Two Degree of Freedom System ($\Omega = 5$)
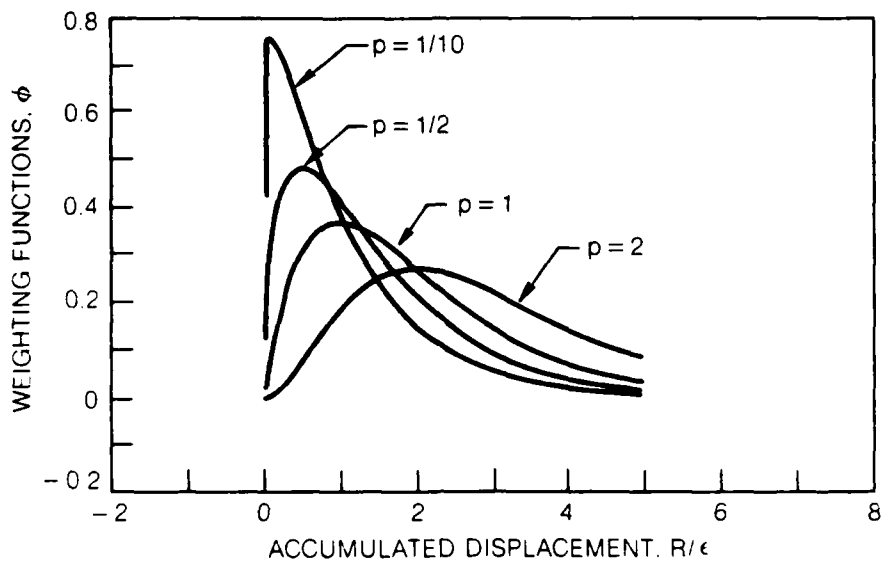
Figure 13 Weighting Function Along Direction of Motion (see Eq. 2.14)
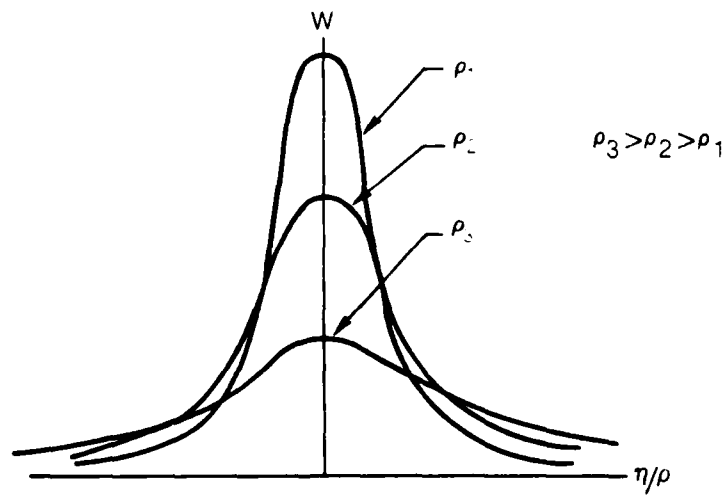
Figure 14 Weighting Function Perpendicular to Direction of Motion (see Eq. 2.15)
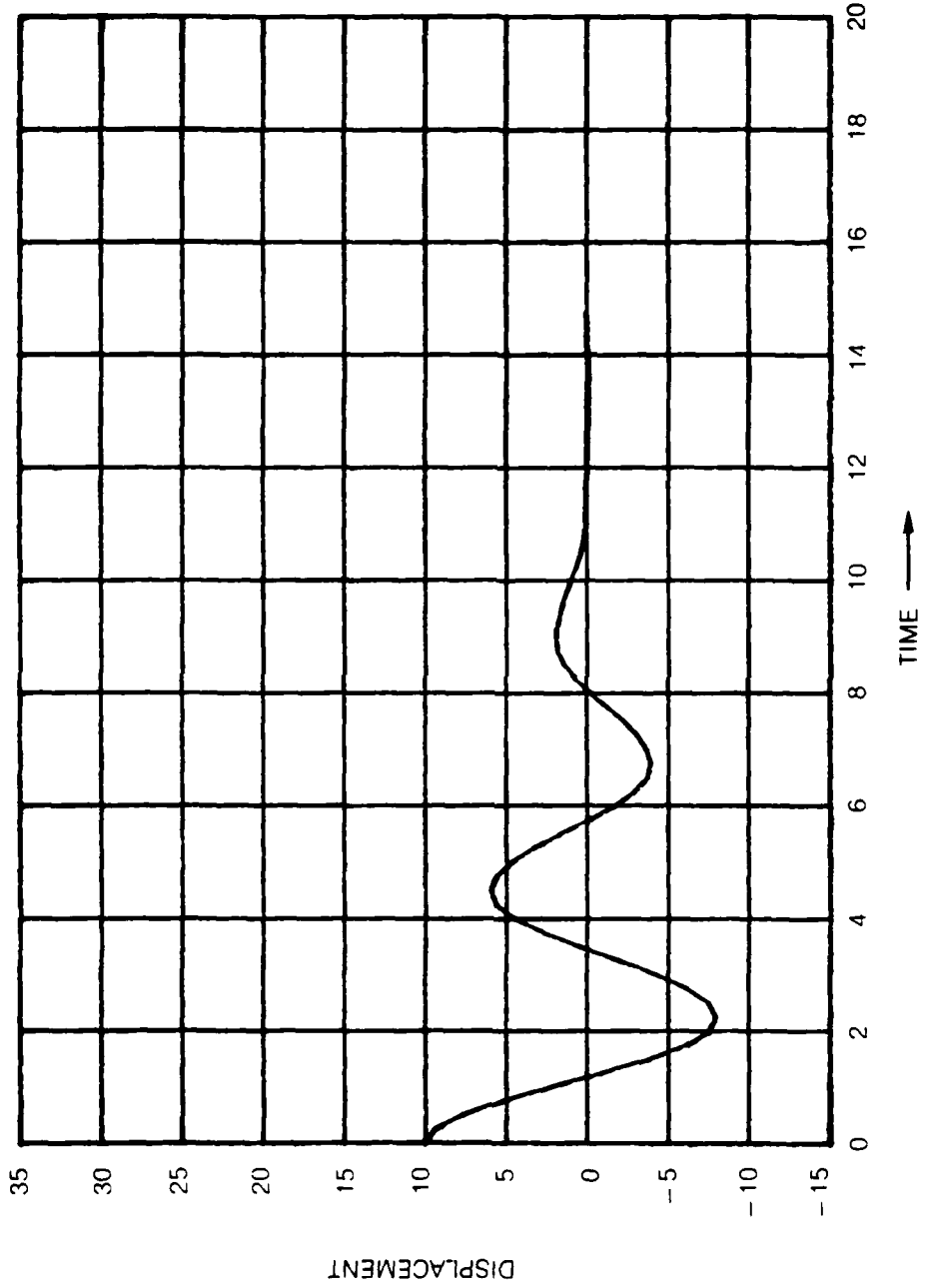
Fig. 15 Displacement History for Single Degree of Freedom Test Case
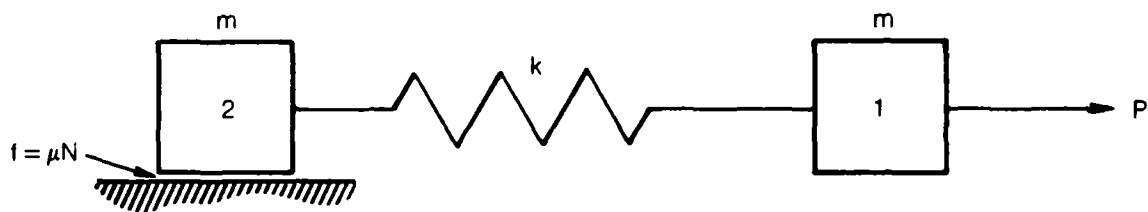
Fig. 16 Two Degree of Freedom
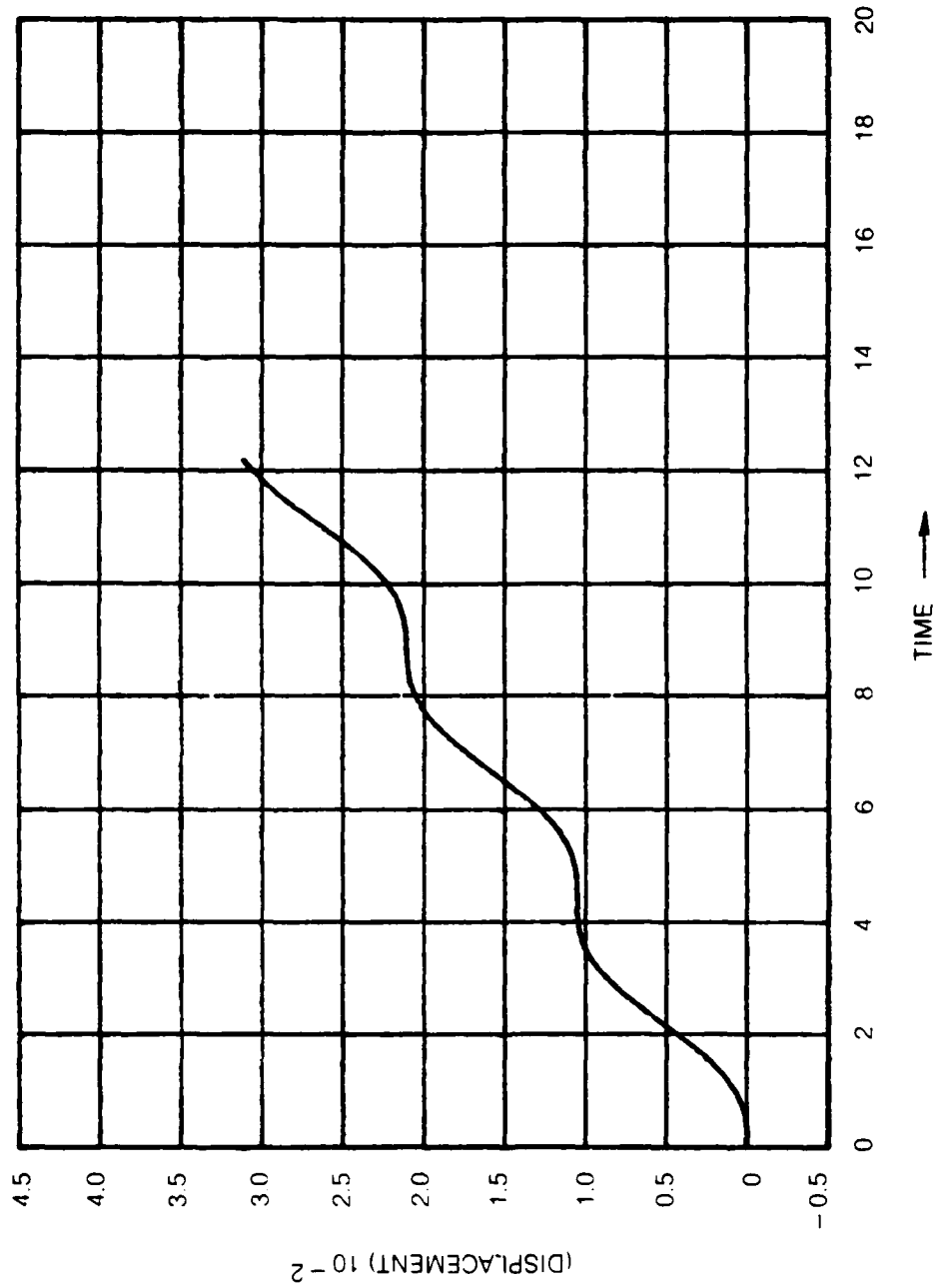
Fig. 17 Displacement of Mass 2 Using Coulomb Friction Law and Displacement Convergence Test

Chart: DISPLACEMENT (10⁻²) vs TIME, with y-axis labeled $(DISPLACEMENT)\ 10^{-2}$ ranging from -0.5 to 4.5 and x-axis labeled TIME ranging from 0 to 20.

85—4—55—2
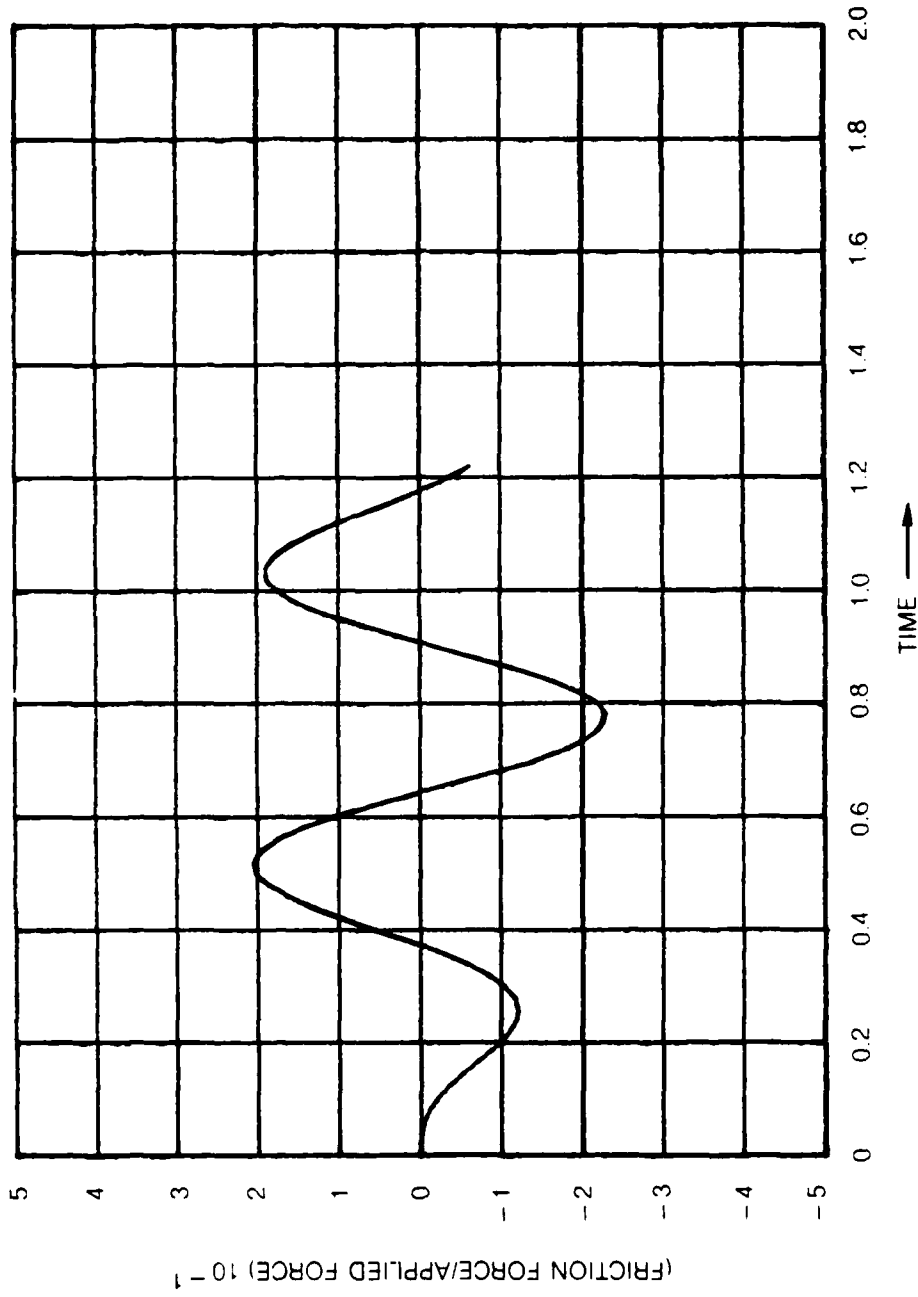
Fig. 18 Friction Force Using Coulomb Friction Law and Displacement Convergence Test

85-4-55-3
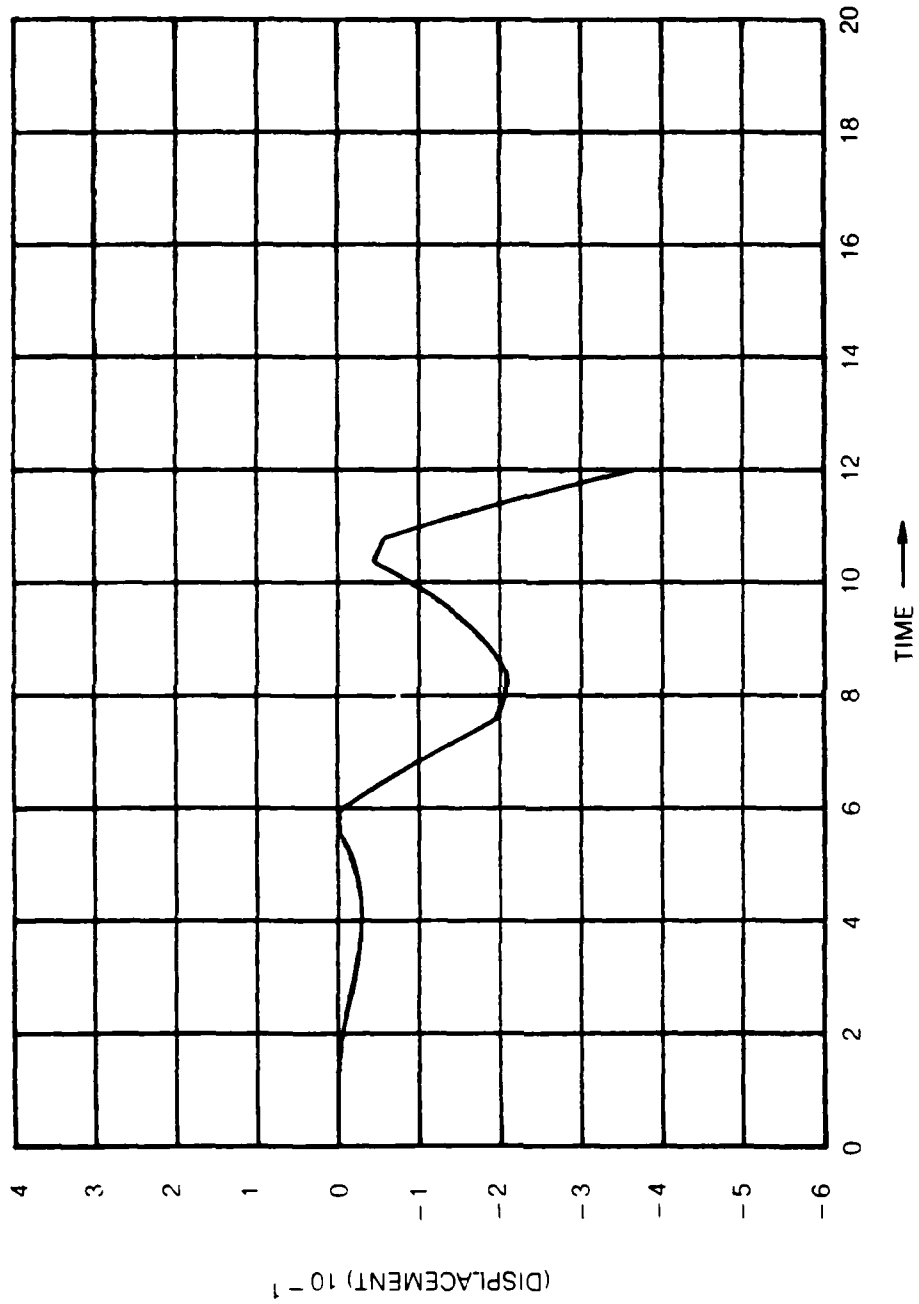
Fig. 19 Displacement of Mass 2 Using Coulomb Friction Law and Velocity Convergence Test
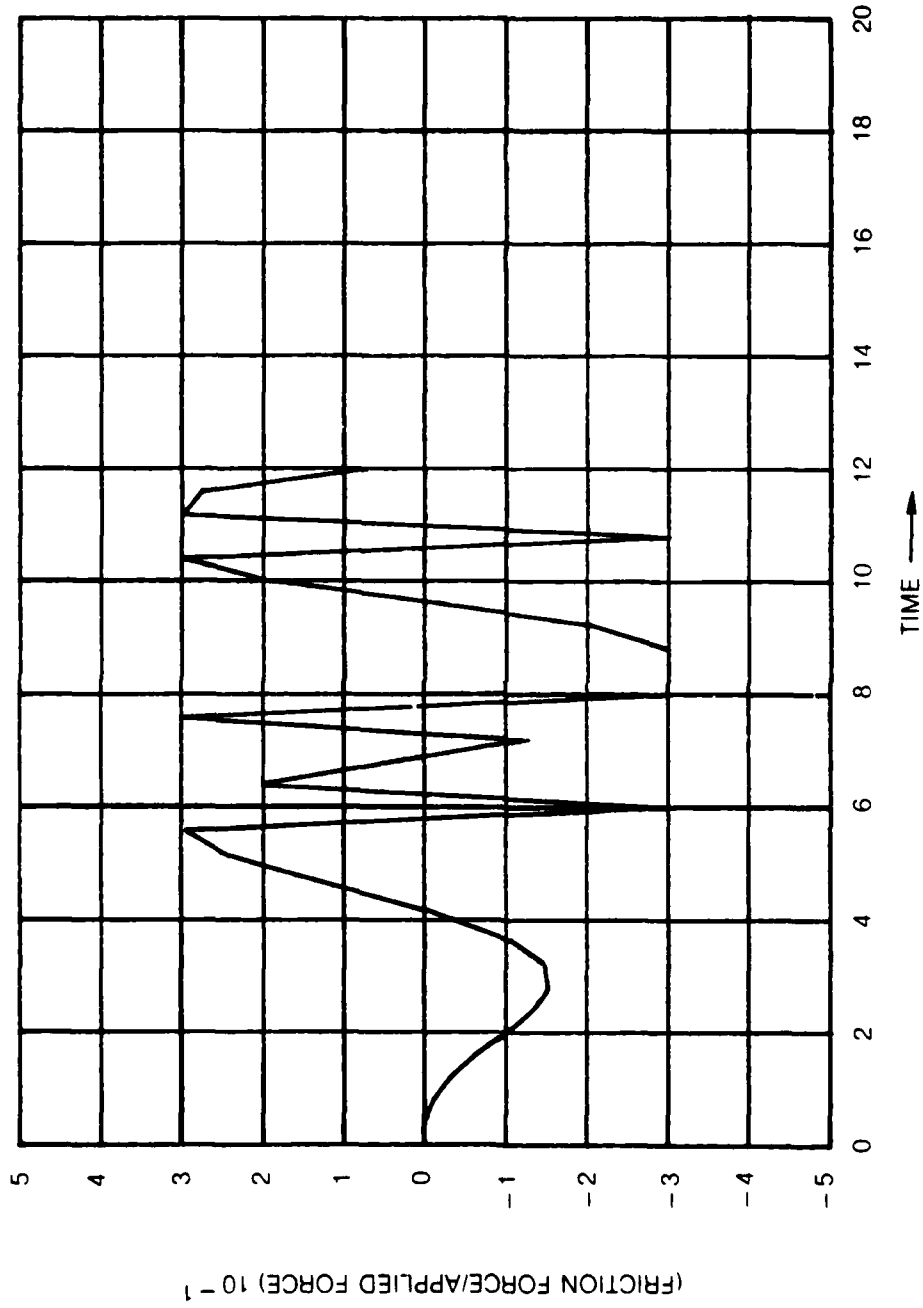
Fig. 20 Friction Force Using Coulomb Friction Law and Velocity Convergence Test

(FRICTION FORCE/APPLIED FORCE) 10^{-1}

TIME ⟶
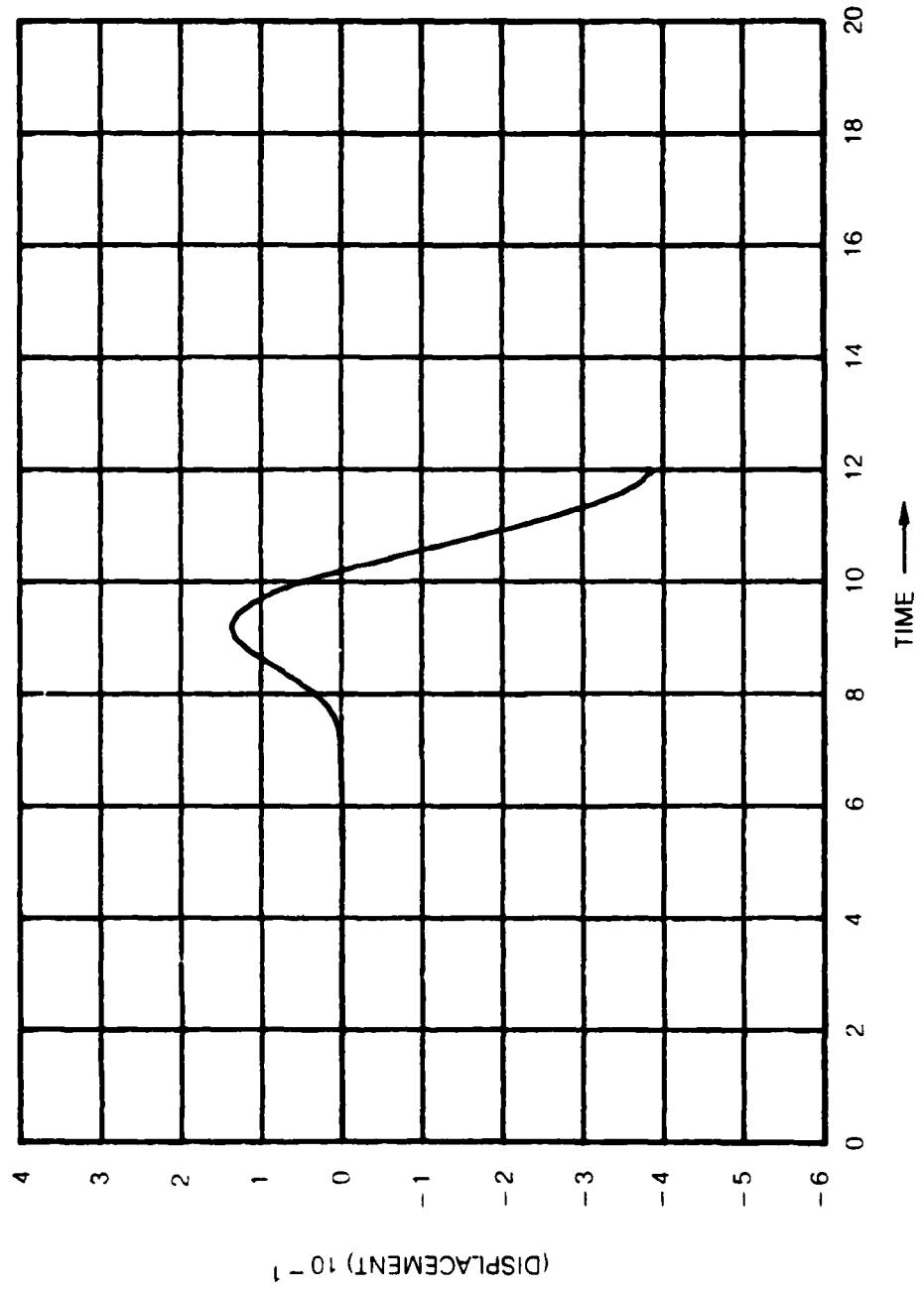
Fig. 21 Displacement of Mass 2 Using Elastic-Plastic Friction Law and Velocity Convergence Test

85—4—85—6
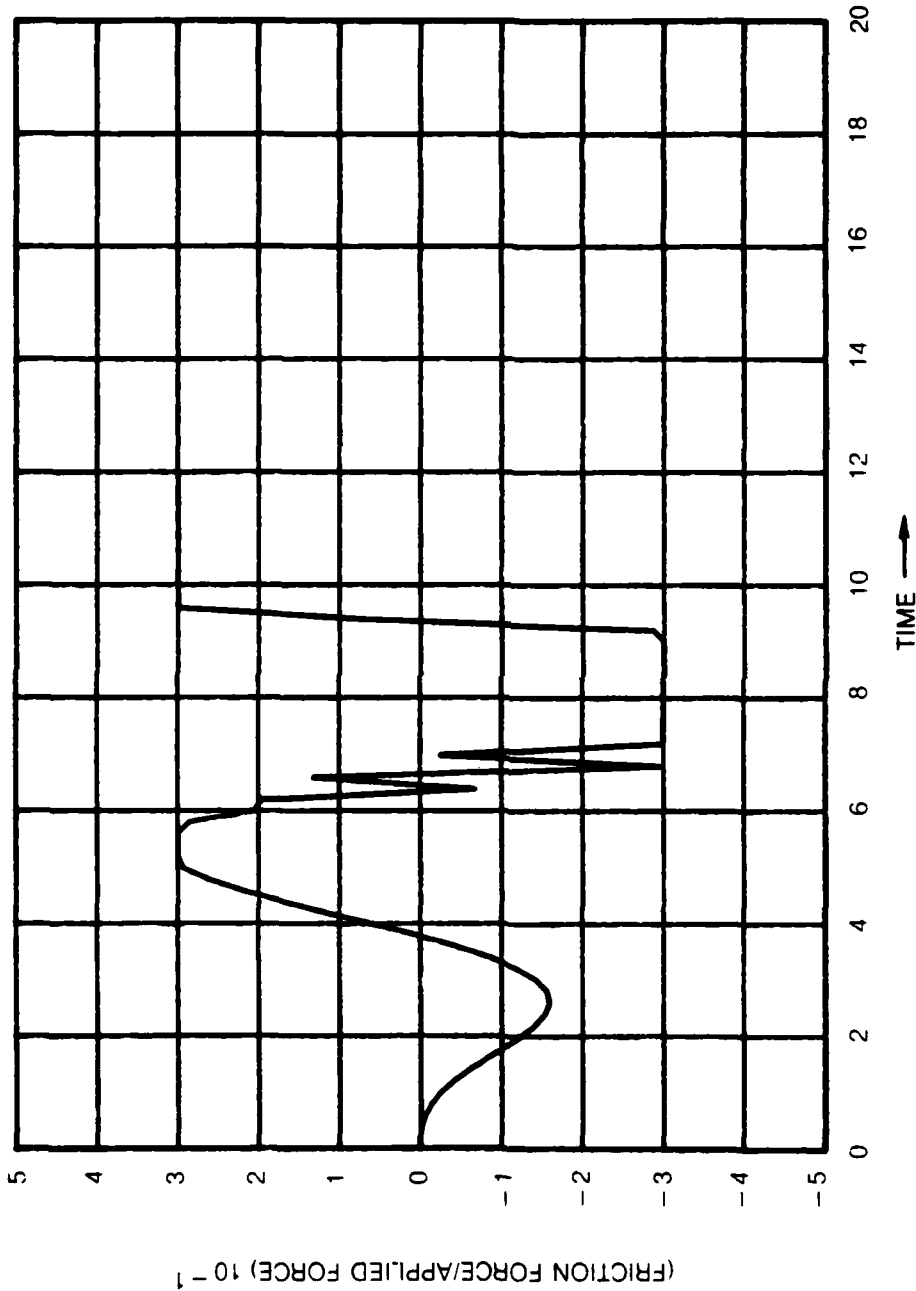
Fig. 22 Friction Force Using Elastic-Plastic Friction Law and Velocity Convergence Test

(FRICTION FORCE/APPLIED FORCE) 10^{-1}

TIME ⟶

MOVING BLOCK
RESPONSE ACCELEROMETER
CONNECTING ROD
FLEXURE
FIXED BLOCK

STRAIN GAGES (TYP)

THERMOCOUPLE LEADS

CABLE (TO APPLY NORMAL LOAD)

SHAKER
SLIP PLATE
INPUT ACCELEROMETER
SUPPORT RAIL
UPPER TEST PIECES
LOWER TEST PIECES
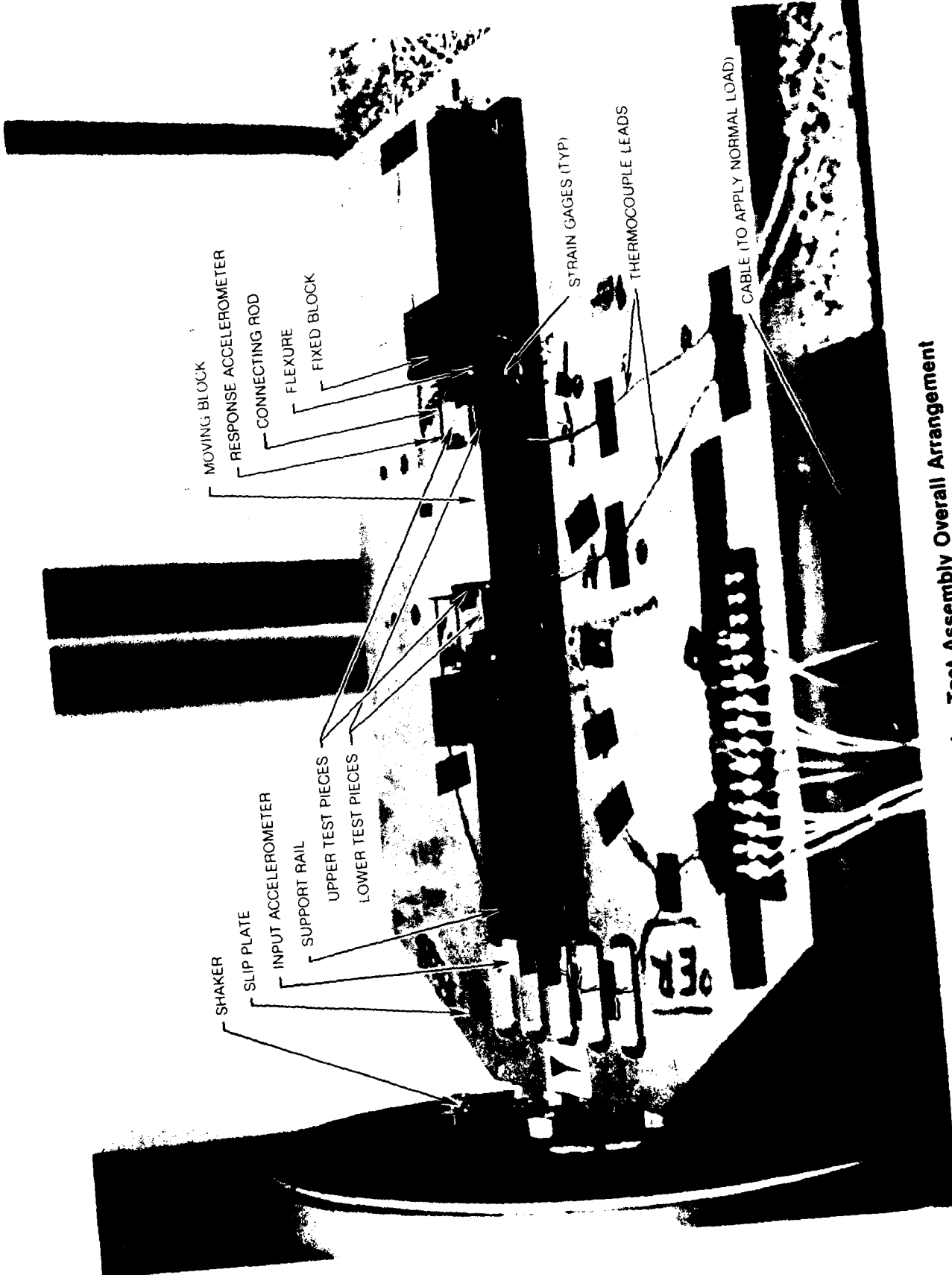
Fig. 23 Friction Test Assembly Overall Arrangement

85—4—69—1

STRAIN GAGED FLEXURES

THERMOCOUPLE LEADS

CONNECTING ROD

LOWER TEST PIECE

UPPER TEST PIECE

MOVING BLOCK

SUPPORT RAIL

FIXED BLOCK
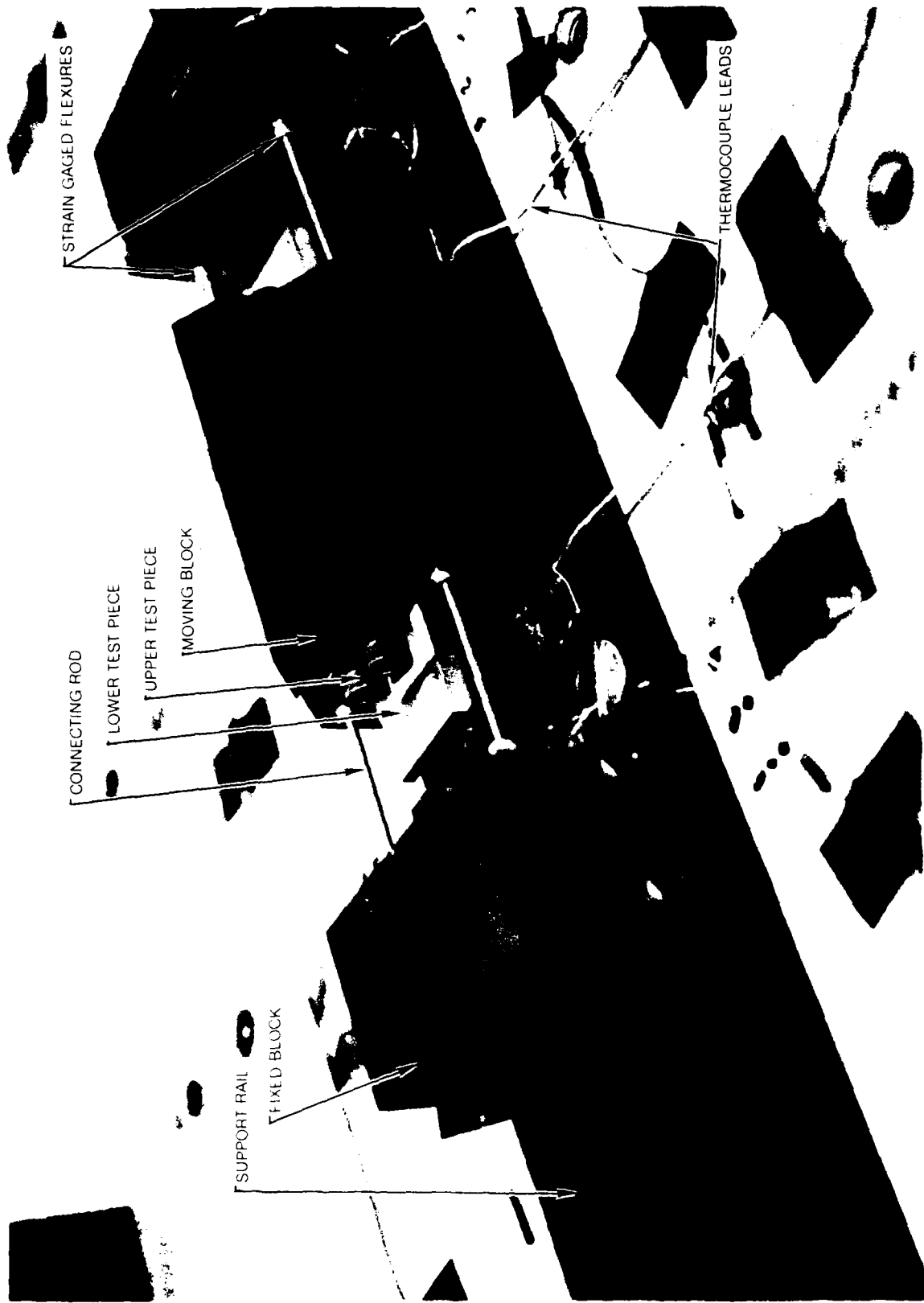
Fig 24 Friction Test Assembly Showing Test Pieces

85-4-69-2

a) UPPER TEST PIECE

DRILL THROUGH 2 HOLES
#8 (0.199 DIA)

THESE SURFACES COATED WITH
0 006 THICK TUNGSTEN CARBIDE
HARDFACE

DRILL THROUGH 4 HOLES #8 (0 199D)
82° COUNTERSINK TO 0 42 MAX DIA

DRILL #38 (0 1015)
0 18 DEEP

(INCH UNITS)

b) LOWER TEST PIECE
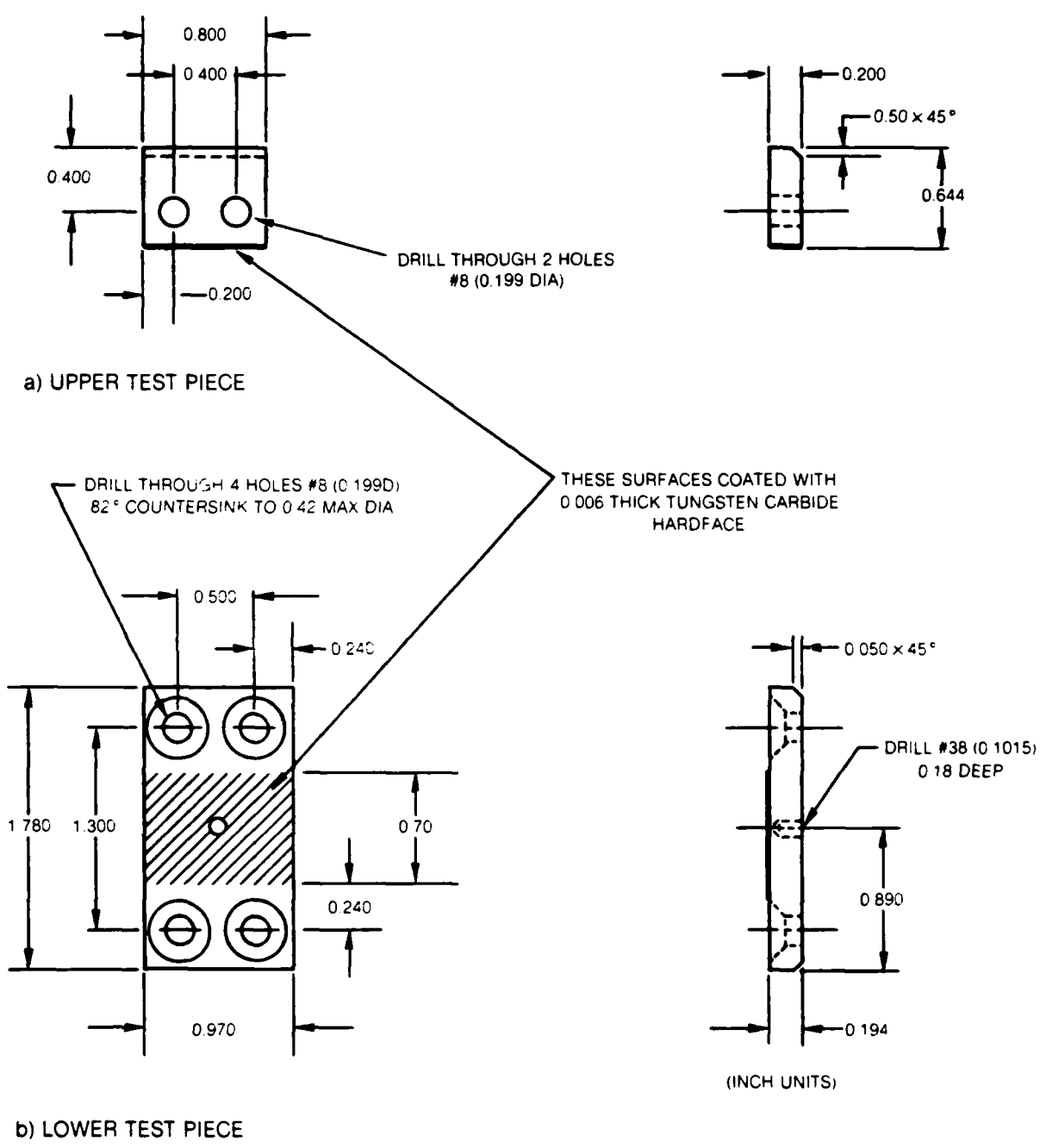
Fig. 25 Details of Titanium 8-1-1 Test Pieces

85—4—69—3

Fig. 26 Frequency Response Function for Axial Motion of Moving Block with No Rubbing

FREQRESP-BODE
1X +   2X +
041585-000000

FREQUENCY (Hz)

143 Hz
+1

73 Hz
+2

2.56E 02

5.00E 01

1.00E 04

1.00E 00

SDOF FRICTION RIGS

INERTANCE (Ins/sec²/Lb)

INERTANCE (Ins/sec²/Lb)

1.00E 03

1.00E-01

5.00E 01

167 Hz

FREQUENCY (Hz)

2.56E 02
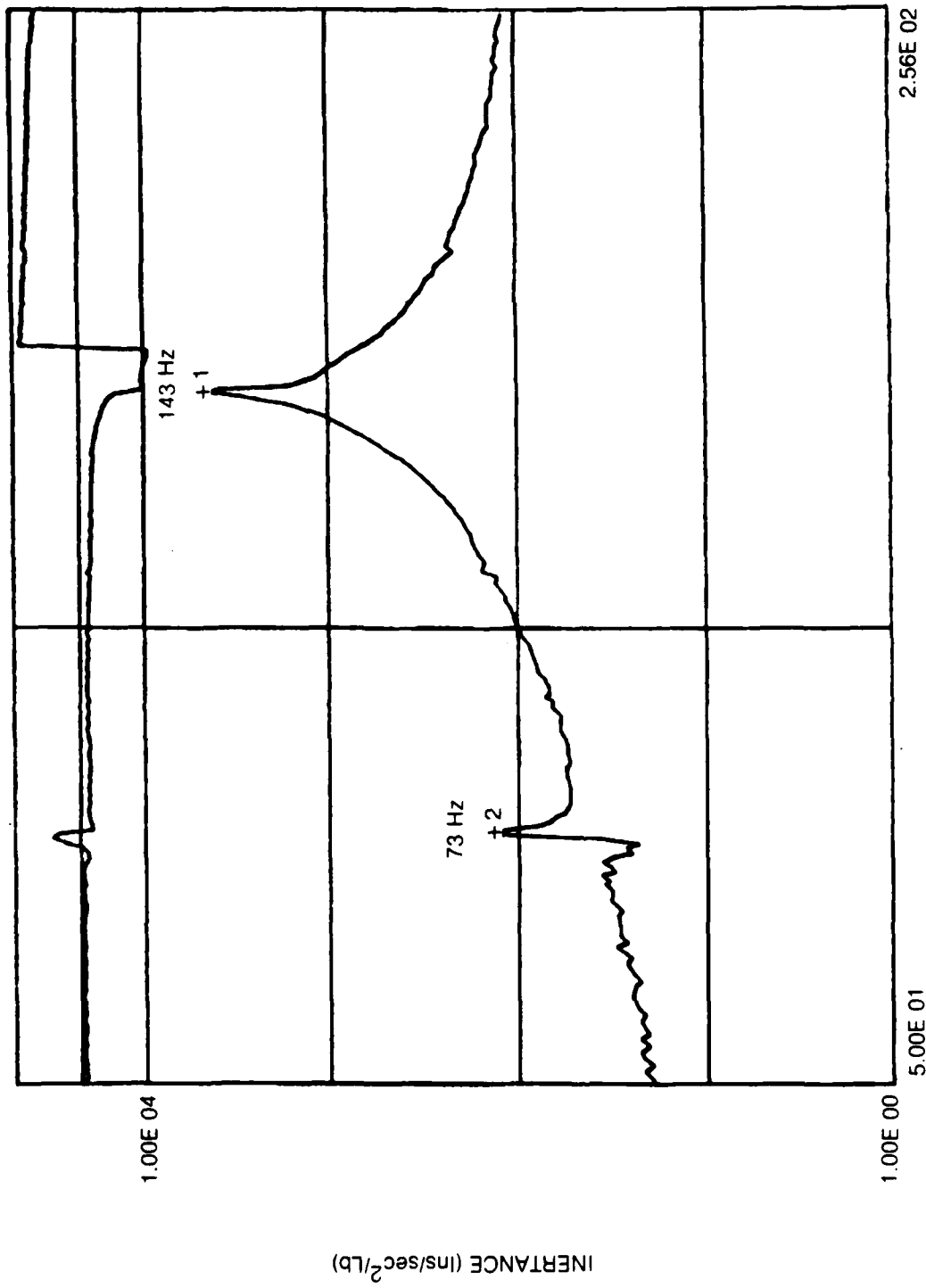
SDOF FRICTION RIGS
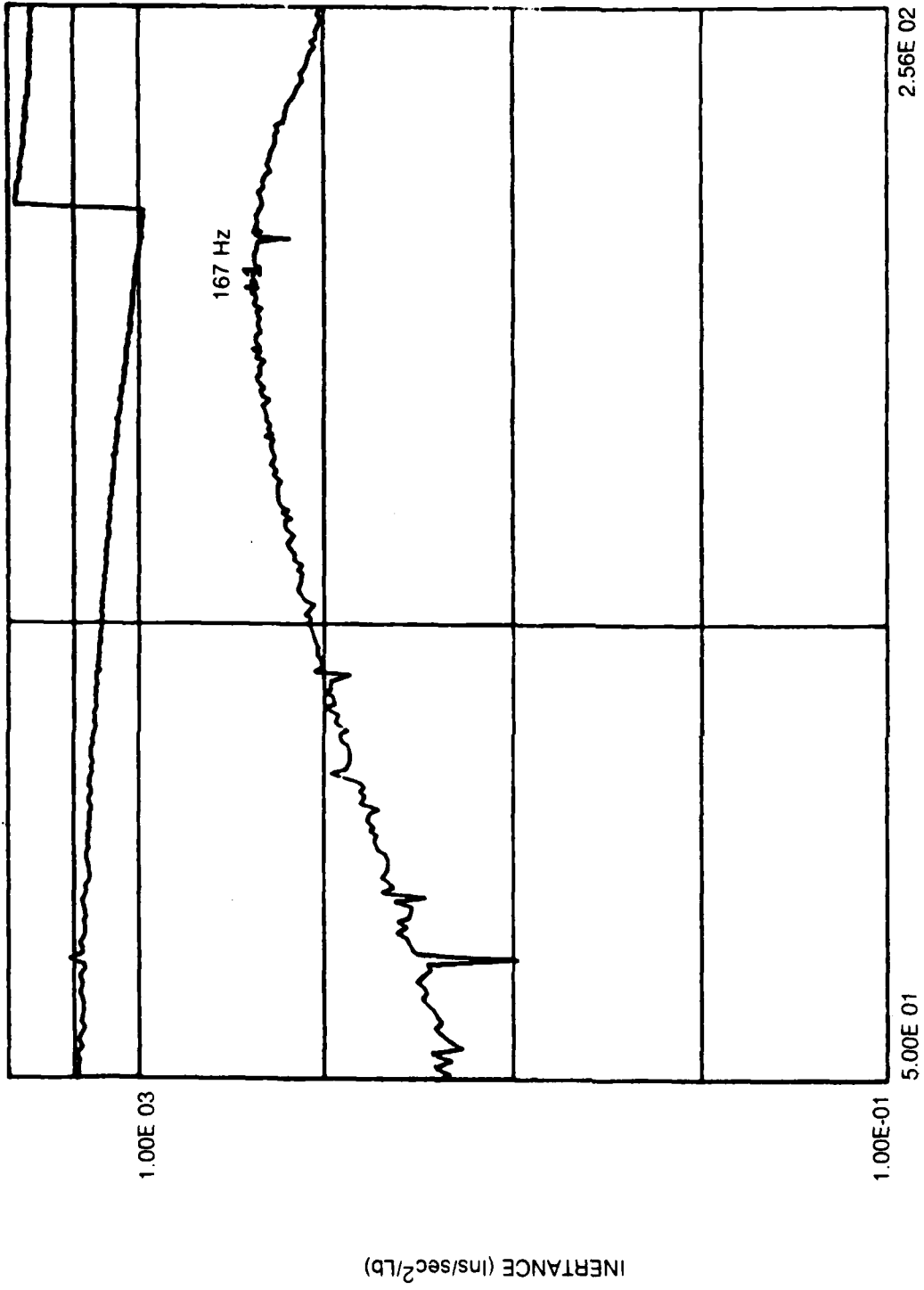
FREQRESP-BODE
1X + 7X +
041585-000000

Fig. 27 Frequency Response Function for Axial Motion of Moving Block with 28 lb Normal Load

85—4—55—15
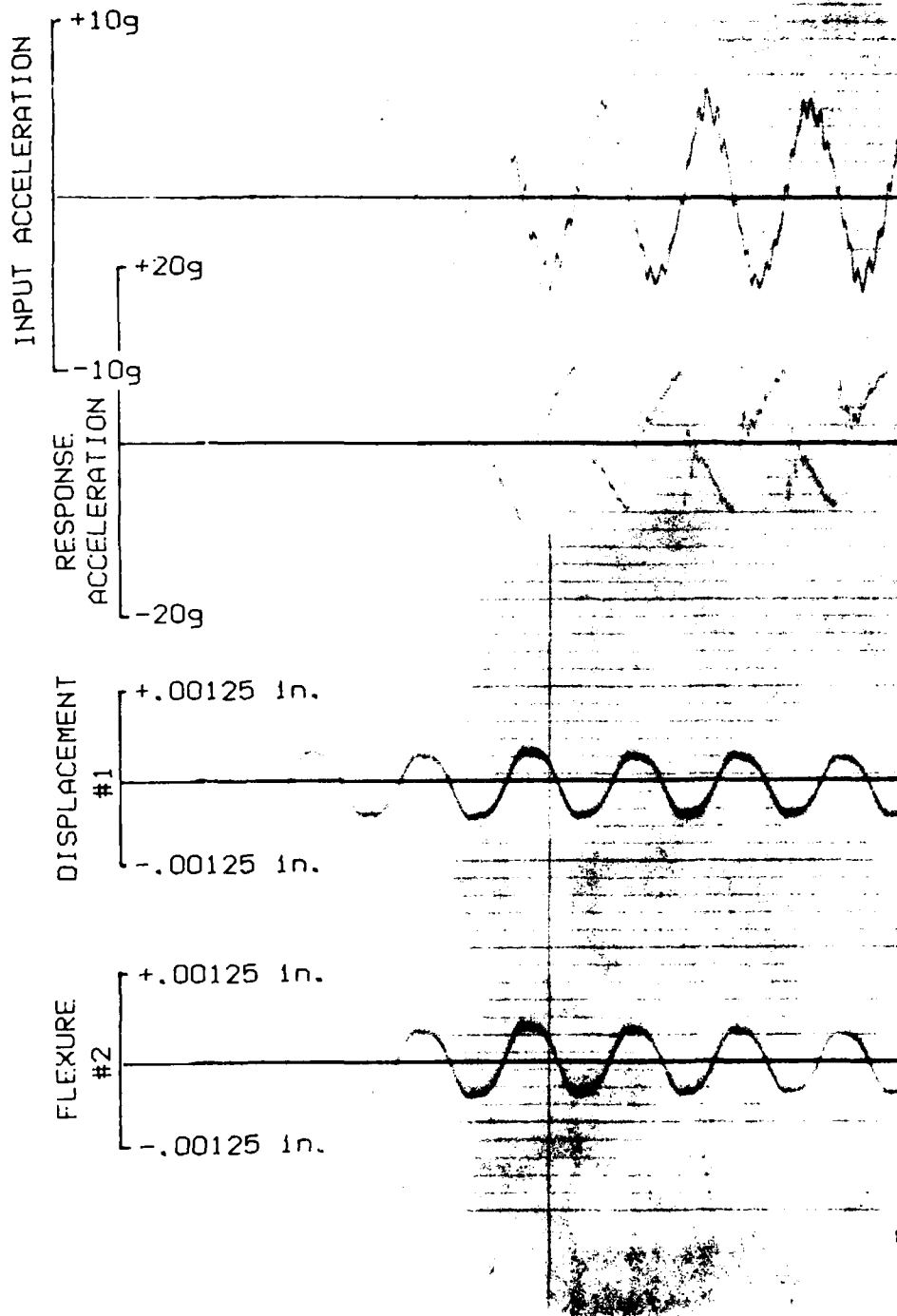
Fig. 28 Typical Time Histories From Friction Test for 135 Hz Input at 5g
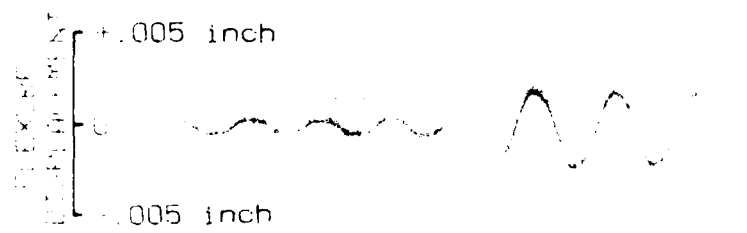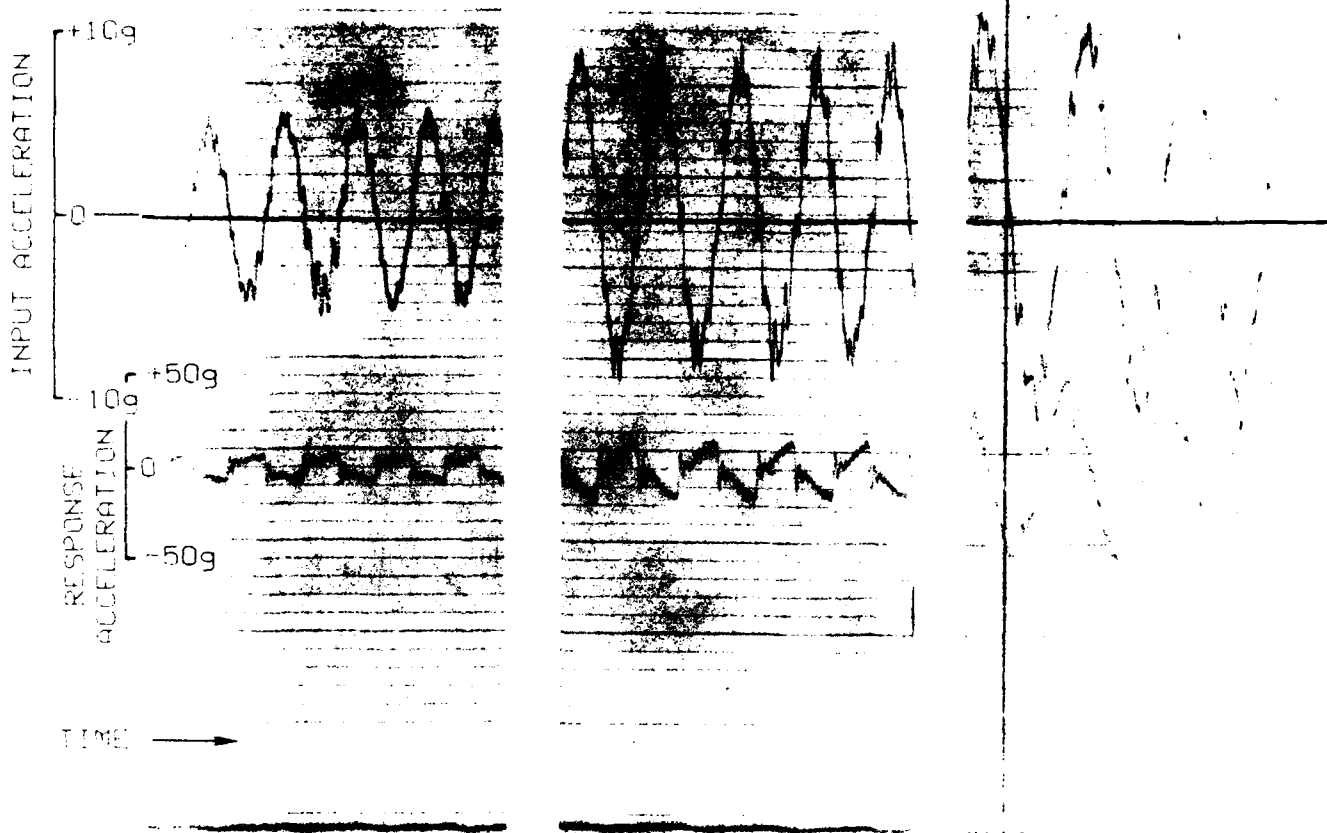
Figure 29 Typical Time Histories From Friction Test for 143 Hz Input
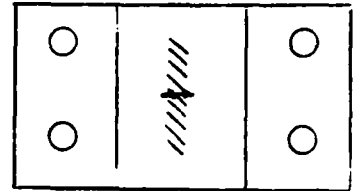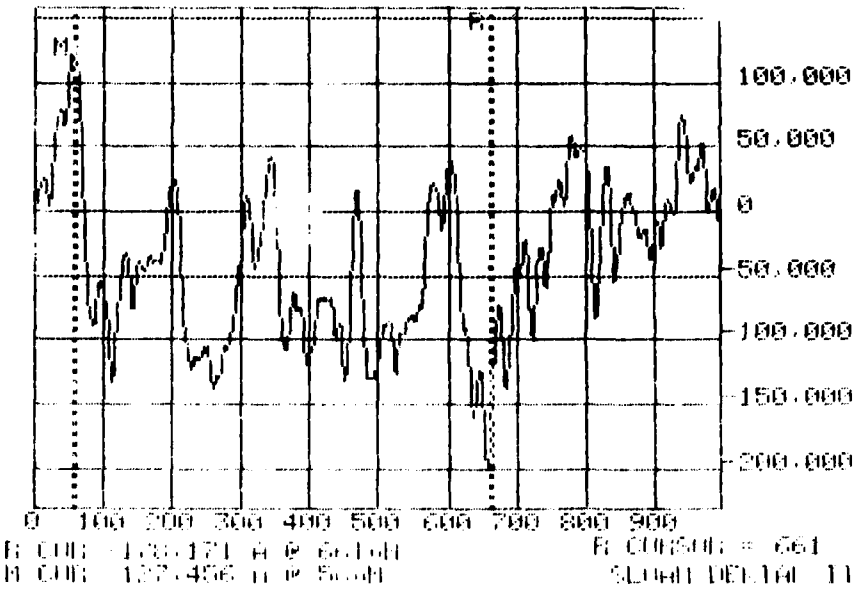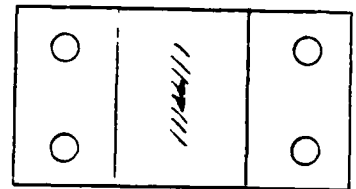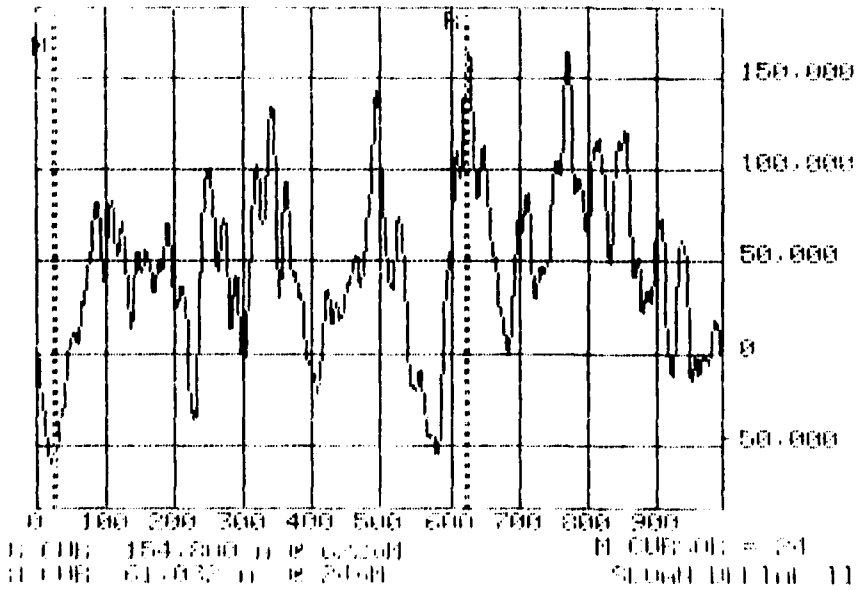
Fig. 30 Profilograms of Center of Contact Area on Lower Test Piece Before Testing
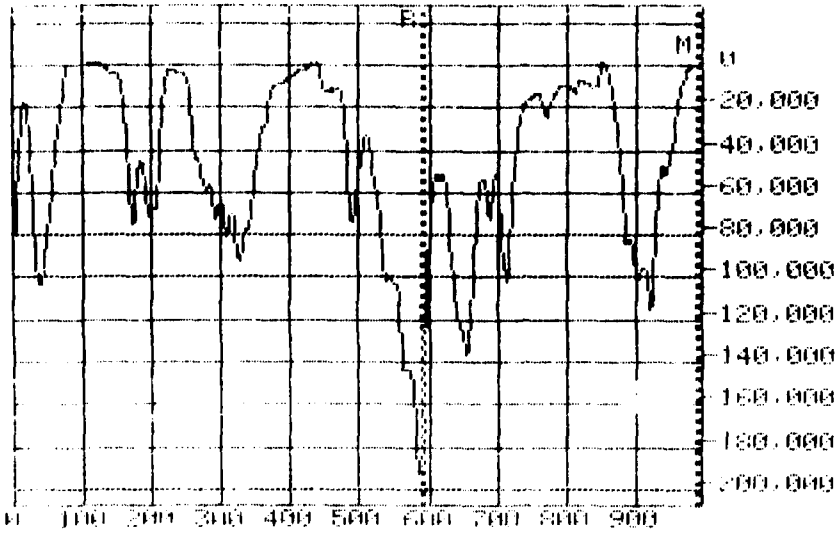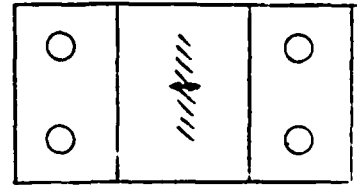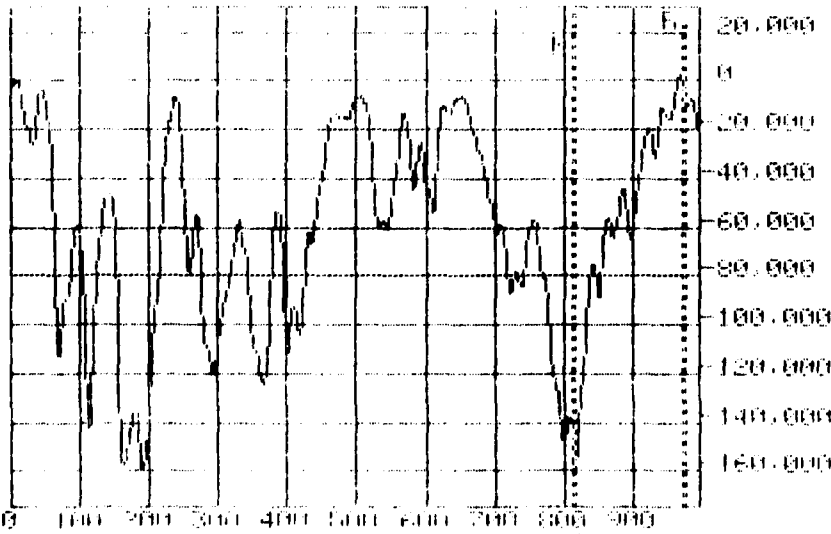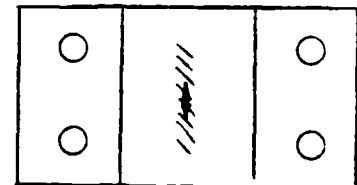
Fig. 31 Profilograms of Center of Wear Area of Lower Test Piece After Testing
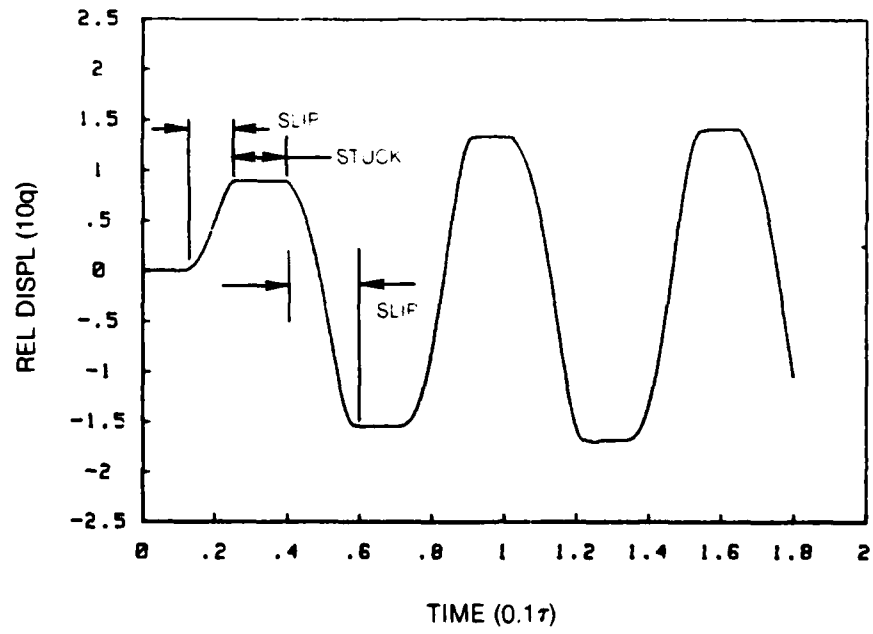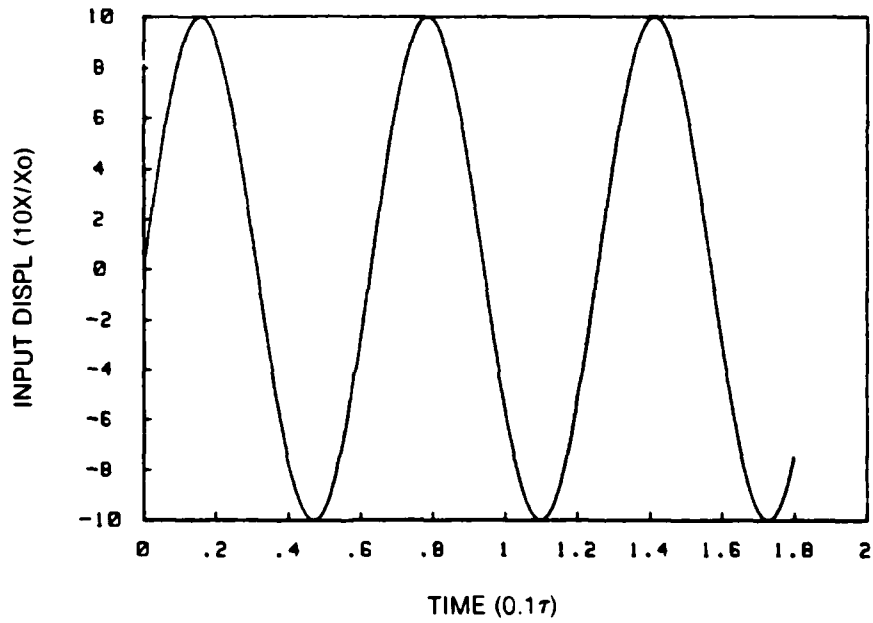
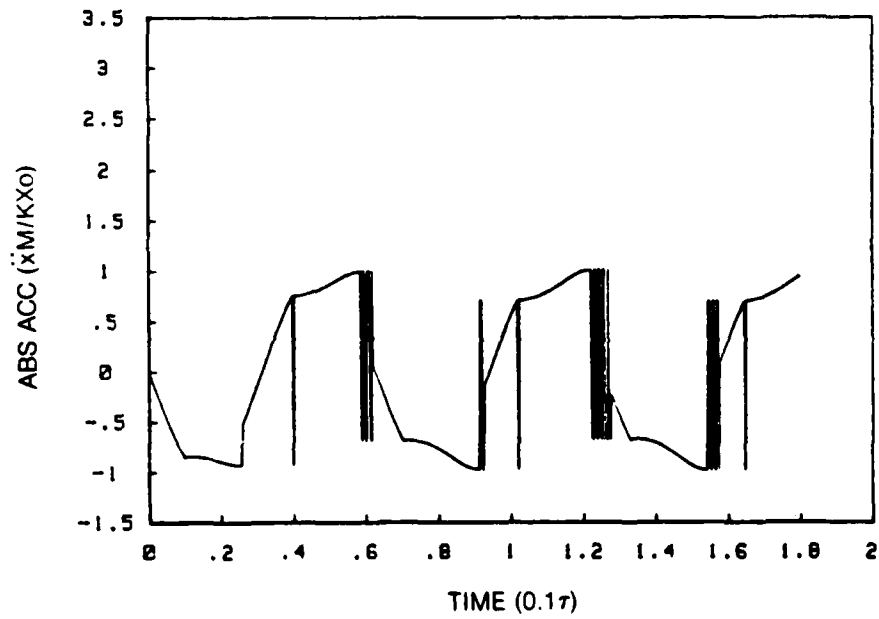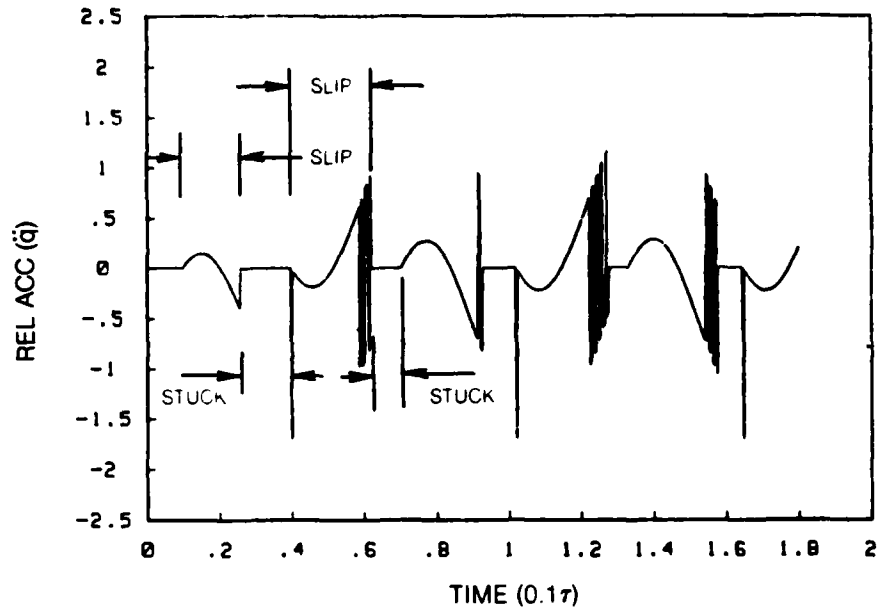**Fig. 32 Expanded Time Histories for S.D.O.F System Analysis**

Fig. 33 Expanded Time Histories for S.D.O.F System Analysis (Continued)

END
FILMED

6-86

DTIC